Supplementary Information for

Composing RNA nanostructures from a syntax of RNA structural modules

Cody Geary, Arkadiusz Chworos, Erik Verzemnieks, Neil R. Voss and Luc Jaeger*

.

*Correspondence to: jaeger@chem.ucsb.edu: Phone: 805 893 3628; Fax: 805 893 4120

This PDF file includes:

1. Materials and Methods
2. Table S1
3. Figs. S1 to S16
4. Additional references

1. Materials and Methods

Structural RNA design

The process of design and nano-construction of RNA nanostructures with RNA structural modules (Figure S1) is described in Figure S2. The various steps are indicated, as well as the software tools used at each step. In Step A, the design of a particular shape is approximated as a network (A.1) according to a set of structural constraints (especially kinks and stacks (A.2)) dictated by the topology of natural RNA modules (specified by nodes) identified in known X-ray structures of RNAs from the protein data bank (http://www.rcsb.org). The edges between nodes indicate the positions of helical struts and interacting RNA modules (A.3) (e.g. loop-loop kissing complexes or tail-tail interactions). In step B, possible candidates of RNA modules that fulfill the structural constraints imposed by the network are selected. In step C, the selected RNA 3D modules specifying for kinks and stacks are joined with helices and interacting modules using Swiss-Pdb Viewer (http://spdbv.vital-it.ch/). The merged RNA fragments are then refined to fix the backbone stereochemistry at the locations of the splices with Assemble 2.0 (http://bioinformatics.org/assemble/) and UCSF Chimera (http://www.cgl.ucsf.edu/chimera/). During this process, the number of base pairs in helices, which represent edges in the network, is adjusted to maximize the formation of the overall shape of the network (C.1 and C.2). The number of units in the final nanostructure is determined by the positions and number of interacting modules (KL or tail-tail) introduced within the network (C.3). Finally, the position of the 3' and 5'end can be specified at the level of some units by the introduction of additional RNA modules promoting helical stacks (C.3). In step D, once a full atomic model is generated, the strand sequence corresponding to each RNA unit is designed by taking advantage of the sequence patterns corresponding to each selected RNA module. Its fold into a unique 2D structure is optimized in order to minimize alternative folds using NUPACK and the Vienna 2.0 package.

The design of the G3-heart is derived from the G2-heart by encoding the six G2-heart units (or domains) into a unique strand (Figures S8 and S16). As an additional design criterion, the folding pathway was chosen in order to favor the local formation of modular RNA subdomains while minimizing the length of transient single stranded regions. In the G2-heart, the RNA units C, E and F are structurally more complex than RNA units A, B and D. After localizing the 5'-3' end of the RNA strand in unit A, the putative pathway of the G3-heart (among a total of 14 different pathways) theoretically leads to the local fold of RNA units C, E and F, while also minimizing the length of transient single stranded regions during transcription to a greater extend than the other pathways. In the final G3-heart model, the tail-tail triple interaction and four of the six KLs interactions are substituted by regular helices. Additionally, the 5' and 3' ends of three units (C,E,F) are capped by UNCG loop modules (Figure S8).

Synthesis of DNA template and RNA units

Synthetic oligonucleotides used as antisense, forward and reverse primers and gblock DNAs were ordered from IDT. Typically, double strand DNA templates were synthesized from antisense DNA template strands or gblock DNA that were amplified by PCR with forward primers, containing the T7 RNA polymerase promoter followed by a sequence complementary to the 5' end of the antisense strand or gblock DNA, and reverse primers, complementary to the 5' end of the sense strand. The length of primer overlap was designed such that the Tm of hybridization to the template sequence was ~56°C. Variations of RNA designs were obtained by primer-induced mutation (which lowers Tm and is compensated accordingly during the PCR thermocycling). All PCR reactions were performed under mineral oil and amplified using Taq DNA polymerase by hot starting at 94°C. PCR reactions were usually carried out in a total volume of 125 for 25 cycles (94°C, 75 sec; 56°C, 75 sec; 72°C, 75 sec). The reaction mixture contained 0.3pmol of template, 150pmol each of both forward and reverse primers with 30μl 5X PCR buffer (250 mM KCl, 50mM Tris pH 8.9, 2.5% NP40, 5mg/mL gelatin) in 2mM $MgCl_2$ plus 60 μM of each dNTP. Following DNA amplification, purification of the PCR products was

performed with a QIAquick PCR purification kit (Qiagen). For RNA synthesis, the entire PCR yield was incubated for 3h at 37°C with T7 RNA polymerase (10 U/μl) in a buffer containing 15 mM $MgCl_2$, 2 mM spermidine, 50 mM Tris 7.5, 2.5 mM of each NTP, 10 mM DTT, 0.01 μg/μl inorganic pyrophosphatase and 0.8 U/μl RNasin to a total volume of 200 μl. The polymerization reaction was quenched by the addition of 3 μl DNase (10 U/μl) and incubation at 37°C for 30 mins. The products of DNA digestion were mixed with denaturing gel loading buffer containing 8 M urea, 20 mM EDTA and purified on 8% denaturing polyacrylamide gel (8M urea) with TBE 1X electrophoresis buffer. RNA products were visualized by UV shadowing and cut from the gel, eluted overnight at 4°C in 300 mM NaCl, 10 mM Tris pH 7.5, 0.5 mM EDTA buffer. The RNAs were precipitated in 1.5 volumes of pure ethanol and washed twice with 90% ethanol. Probe RNAs were 32P labeled at the 3' end by [32P] pCp ligation with T4 RNA ligase and purified on 8% denaturing polyacrylamide gel. For visual monitoring on gels, 1 nM of molecule A or B in the set was radiolabeled (prepared by ligation of a ^{32}P labeled pCp to the 3' end).

RNA folding and self-assembly

Folding Protocol 1: RNAs are prepared by mixing different programmable tectoRNAs (200 nM each, unless otherwise specified) in water. RNA samples were subjected to a denaturation/renaturating step by heating the samples to 90°C for 3 mins, cooling on ice 3 mins, incubation at 30°C for 3 mins, followed by addition of 5X concentrated buffer to reach 10 mM Tris-borate pH 8.2 (TB), 50 mM KCl, and 0.2 mM $Mg(OAc)_2$, prior further incubation at 30°C for 30 mins.

Folding protocol 2: in addition to protocol 1, RNA nanostructures were further stabilized for native PAGE and AFM studies, through this additional step: the magnesium concentration was raised to 15 mM $Mg(OAc)_2$ by the addition of a 2X concentrated buffer (RNA is diluted to 100 nM) and then further heated at 60°C for 10 min and slow cooled to 10°C over 30 min.

Native-PAGE and TGGE assays

Native PAGE and TGGE experiments were performed essentially as described in reference[1]. For native-PAGE analysis, 10 µl of RNA sample (usually at 100 nM RNA unless specified) was combined with 1 µl of gel loading buffer (0.01% bromophenol blue, 0.01% xylene cylanol, and 20% glycerol) and run on a 5% (38.5:1) non-denaturing PAGE at 50W and 10°C for various times. $Mg(OAc)_2$ (typically at 0.2 mM, 1 mM or 15 mM) was present in both gel and electrophoresis buffer at the specified concentration. For TGGE analysis, the experimental setup was adjusted to have a linear temperature gradient perpendicular to the electric field. The temperature gradient was typically set up from 25°C to 65°C. 20 µl of RNA sample (40 nM RNA squares or triangles) was combined with 2 µl of gel loading buffer and run on 5% (38.5:1) native PAGE at 20 W for 1 hr. $Mg(OAc)_2$ (typically 0.2 mM) was present in both gel and electrophoresis buffer.

Structural probing of RNA

Lead-induced cleavage: RNAs were assembled *via* protocol 1. Chemical and enzymatic probing were all performed at various concentrations of Pb(II) on unit Y alone or within the context of the G1-heart, in absence or presence of 1mM AMP. Lead acetate (EMD) solution (80 mM) was prepared daily to avoid degradation. The reaction mixture consisted of unit Y (400 nM) or G1-heart (200 nM), association buffer (15 mM $Mg(OAc)_2$, 25 mM K(OAc) and 25 mM HEPES, pH 7.5), and 1 μl yeast tRNA (10 mg/mL). The cleavage reaction was initiated after adjusting the reaction mixture (10 μl) to various final concentration of $Pb(OAc)_2$ (16 to 42 mM) and incubated for 5 min at 25°C. To quench the reaction, 5 μl of 0.1 M EDTA was added to the reaction mixture followed by ethanol precipitation. The RNAs were precipitated in EtOH at –20°C for 1 hour and washed twice with 90% EtOH, dried, and then reconstituted in gel loading buffer. The RNA fragments were separated on denaturing polyacrylamide gels (15% acrylamide 29:1, 8 M urea). As a control ladder, RNase T1 probing was performed according

to the manufacturer recommendation and all the enzymes and buffers were purchased from AMBION®.[1,2] Alkaline hydrolysis ladders of unit Y were obtained by incubation at 95°C for 10 min in presence of 50 mM sodium carbonate pH 9.2, 1 mM EDTA and 1 μg of yeast tRNA. Reaction volumes of 10 μl were directly loaded onto the gel after addition of blue/urea buffer.

Atomic force microscopy (AFM)

Tectosquare and tectotriangle arrays and 2X2 Grids: For AFM imaging, various combinations of tectosquares or tectotriangles (typically at 5 nM each) were first mixed at 4°C in TB, 15 mM $Mg(OAc)_2$, 50 mM KCl, before deposition on the surface of the freshly cleaved ruby mica (S&J Trading Inc., Glen Oaks, NY) at 50°C. Nanostructure assembly was then performed by slow cooling from 50°C to 4°C in 16 hours. The composition of each nanostructure used in this study is indicated Table S1. Tectosquares for 2X2 Grids were prepared according to RNA folding protocol 2. The two squares (I and II) were then mixed to a final concentration of 6nM of each square in 15 mM $Mg(OAc)_2$ TB, and 50μL of the mixture were deposited on pre-warmed mica (40°C). The RNAs were then slow annealed on the mica surface from 40°C to 4°C over 16h. AFM images were collected in tapping mode under 15mM $Mg(OAc)_2$, TB buffer solution using a Digital Instrument Nanoscope IIIA Model NS-3 and J-scanner.

TT5-TT6-TT7 triangles: Triangle assemblies were prepared according to RNA folding protocol 2. TT5, TT6 and TT7 were then mixed to a final concentration of 3 nM each in a solution of 100 mM $MgCl_2$. Mica surfaces were pre-treated with 100 mM $NiCl_2$ for 15 min. 50 μL of triangle assembly was deposited onto the mica for 15 min, and then washed 3 times with HPLC-grade water and dried under N_2. AFM images were collected in tapping mode under continuous flow of N_2, using a Digital Instrument Nanoscope IIIA Model NS-3 and E-scanner.

G1 and G2 hearts: RNA hearts were prepared according to RNA folding protocol 2. G2-heart dimers were similarly prepared, except that the two programmable tail units (A1-t1a + A1-t1b or A2-t1a + A2-t1b) were added at 100nM concentration each to obtain a 1:2 stoichiometry with the other RNA units (B,C,D,E,F). AFM images were collected in tapping mode under 15mM $Mg(OAc)_2$, TB buffer solution using a Digital Instrument Nanoscope IIIA Model NS-3 and J-scanner. Images in air (under flow of nitrogen) were collected with NSC12 (now NSC35) silicone probe with typical resonance frequency f=140–210 kHz and spring constant k=4–9 N/m, except the one obtained with NSC14/Hi-Res-C probe (now upgraded to Hi'Res-C14/Cr-Au) with resonance frequency f=150 kHz and spring constant k=4 N/m. For images collected under liquid (10 mM TB pH 8.2, 50 mM KCl 15 mM $MgCl_2$) the MSNL-10 (cantilever C or D) silicone probe on silicone nitride lever with typical resonance frequency f=5–20 kHz were used. A typical scan range was 500-2000 nm. Images were processed and analyzed using NanoScope or Gwyddion software. Raw data were leveled by a first and second order plane fit correction to remove the sample tilt. Contours of the high-resolution AFM images of G2-heart particles obtained with Hi'Res-C14/Cr-Au probes (Fig. 3F,G and Fig S13e) were generated using the MatLab software, and more specifically its image analysis module, which interpolates and smoothens AFM data.

G3-heart co-transcriptional folding and AFM visualization

Freshly-cleaved mica affixed to a metal disk was preheated to 37.0°C and set aside. RNAs were co-transcriptionally folded in one-pot reactions. Template DNA (4 ng/μl final) was added to a reaction mix buffer containing 6 mM $Mg(OAc)_2$, 40 mM Na-OAc, 40 mM KCl, and 50 mM Tris-OAc (pH 7.8). NTPs (0.5 mM each final) and DTT (1 mM final) were added prior to the addition of T7 RNA polymerase (~0.2 U/50 μl). Transcription reactions were carried out in 50 µl volumes at 37.0°C for 20 minutes. For AFM imaging, 5 μl of the transcription mix was directly mixed with AFM buffer (12.5 mM $Mg(OAc)_2$, 40 mM KCl, 40 mM NaCl, TB pH7.8) on mica surface. The mica was then vigorously rinsed after 1minute by removing the fluid and addition of fresh AFM buffer (40 μl) and 4 μl of 60 mM $NiCl_2$. Multimode imaging was performed with 9.7khz "solution imaging" tips under these AFM buffer conditions.

Cryo-electron microscopy

Sample Preparation for Cryo-Electron Microscopy: RNA samples were prepared for Cryo-EM imaging by the same protocols used to generate AFM samples. RNAs were suspended in 15 mM $Mg(OAc)_2$, 50 mM KOAc TB buffer. Samples were packed on ice and shipped via next day delivery to the Scripps Research Institute and imaged at the National Resource for Automated Molecular Microscopy.

Cryo-EM protocol for imaging G2-hearts: Samples were preserved in a thin layer of vitreous ice supported by a thin layer of carbon on 2.0 x 0.5 μm C-Flat holey carbon films (Protochips, Inc.) Grids were cleaned immediately prior to use in a Solarus plasma cleaner (8 seconds, 25% O2, 75% Ar). A drop (~3 μl) of the undiluted sample suspension was applied to a plasma-cleaned grid, blotted away with filter paper and the sample was immediately vitrified in liquid ethane, using an FEI Vitrobot (4C, 95% RH). Data were acquired using a Tecnai F20 Twin transmission electron microscope operating at 120 kV, using a dose of ~30 e-/Å^2 and a nominal underfocus ranging from 1 to 3 μm. All images were recorded with a Tietz F415 4k x 4k pixel CCD camera (15 μm pixel) using the Leginon data collection software[3]. Eighty-six images were automatically collected at a nominal magnification of 80,000X at a pixel size of 0.105 nm at the specimen level. Experimental data were processed using the Appion software package[4], which interfaces with the Leginon database infrastructure. Initially, 4,467 particles were automatically selected from the micrographs using the FindEM[5], template-based particle picker. The contrast transfer function (CTF) was estimated and corrected including astigmatism using ACE2, a variation of the software described in reference[6]. Particles were extracted from the CTF corrected images with a box size of 360 pixels. The set was reduced to 2,456 particles by reference-free alignment and classification and removing any particles that aligned to bad class averages. All alignment and classification was done with Appion toolbox[7] by the Xmipp MLalign2D program[8] using the fast algorithm[9]. A resolution of 20.8 Å for the class average based on the 2,456 particle set was determined by converting the spectral signal-to-noise ratio (SSNR) into a Fourier ring correlation (FRC) taken at a 0.5 cutoff[10].

Acknowledgements

Cryo-EM was performed at the National Resource for Automated Molecular Microscopy, which is supported by the NIH National Institute of General Medical Sciences (GM103310).

2. Supplementary tables

Table S1: Complete list of RNA sequences and composition of nanostructures used in the study.

A. 3WJ-TectoRNA sequences

TectoRNA nomenclature: A, B, C, and D indicate the type of the unit with respect of their KL modules in a clock-wise fashion within the context of the tectosquare (TS) or tectotriangle (TT). When sequence units enter into the composition of a tectosquare or a tectotriangle, the unit number is followed by a lowercase s or t, respectively. For example, A1s enters into the compostion of tectosquares: it is based on the UA_h_3WJ module, the 5' and 3' KL loops are L1 and L2', respectively, and it has a closing stem of 5bp and a 3' tail t1' (see also Figure S1). When units A, B, C, D or T are immediately followed by a lowercase "r", it indicates that the KL interactions have been flipped in order to control orientation of the assembly through tail-tail interactions in other directions. In the table, yellow indicates the position of KLs and green indicates the sequence of tail connector used. Tr unit (flipped T unit) requires 4 extra bp to compensate for distortions. *See also Figure S3 for secondary structures and assembly*.

TectoSquare TS and TectoTriangle TTo	
TS_A0s: 3WJ-L1-L2'-5bp-t0	GGGACGGACAGCGUGCAUGGUGAAGGAGGCACGCCAUGCACGCUGCAGACCGAACGUGAA GUGGACACGCGUUCGGUCUGCUAACGUUCCU
TS_B0s: 3WJ-L2-L3'-5bp-t0	GGGACGGACAGCGUGCAUGGUGAAGUCCACACGCCAUGCACGCUGCAGACCGAACGUGAA GCCUGCACGCGUUCGGUCUGCUAACGUUCCU
TS_C0s: 3WJ-L3-L4'-5bp-t0	GGGACGGACAGCGUGCAUGGUGAAGCAGGCACGCCAUGCACGCUGCAGACCGAACGUGAA GCGAGCACGCGUUCGGUCUGCUAACGUUCCU
TS_D0s: 3WJ-L4-L1'-5bp-t0	GGGACGGACAGCGUGCAUGGUGAAGCUCGCACGCCAUGCACGCUGCAGACCGAACGUGAA GCCUCCACGCGUUCGGUCUGCUAACGUUCCU
TTo_0st: 3WJ-L3-L1'-5bp-t0	GGGACGGACAGCGUGCAUGGUGAAGCAGGCACGCCAUGCACGCUGCAGACCGAACGUGAA GCCUCCACGCGUUCGGUCUGCUAACGUUCCU
TectoTriangle TT and TectoSquare TSa	
TT_A0t: 3WJ-L1-L2'-2bp-t0	GGGCUAACGCAGACCGAUGAAGGAGGCACGUCGGUCUGCGGACAGCCGUGCAUUGAAGUG GACACGAUGCACGGCUGCCCU
TT_B0t: 3WJ-L2-L3'-2bp-t0	GGGCUAACGCAGACCGAUGAAGUCCACACGUCGGUCUGCGGACAGCCGUGCAUUGAAGCC UGCACGAUGCACGGCUGCCCU
TT_T0t: 3WJ-L3-L1'-2bp-t0	GGGCUAACGCAGACCGAUGAAGCAGGCACGUCGGUCUGCGGACAGCCGUGCAUUGAAGCC UCCACGAUGCACGGCUGCCCU
TSa_C0ts: 3WJ-L3-L4'-2bp-t0	GGGCUAACGCAGACCGAUGAAGCAGGCACGUCGGUCUGCGGACAGCCGUGCAUUGAAGCG AGCACGAUGCACGGCUGCCCU
TSa_D0ts: 3WJ-L4-L1'-2bp-t0	GGGCUAACGCAGACCGAUGAAGCUCGCACGUCGGUCUGCGGACAGCCGUGCAUUGAAGCC UCCACGAUGCACGGCUGCCCU
TS constructs	
TS_A1s: 3WJ-L1-L2'-5bp-t1'	GGGACGGACAGCGUGCAUGGUGAAGGAGGCACGCCAUGCACGCUGCAGACCGAACGUGAA GUGGACACGCGUUCGGUCUGCUAACGUUCCCCAGAG
TS_Br1s: 3WJ-L3'-L2-5bp-t3'	GGGACGGACAGCGUGCAUGGUGAAGCCUGCACGCCAUGCACGCUGCAGACCGAACGUGAA GUCCACACGCGUUCGGUCUGCUAACGUUCCCGGUGA
TS_C1s: 3WJ-L3-L4'-5bp-t2'	GGGACGGACAGCGUGCAUGGUGAAGCAGGCACGCCAUGCACGCUGCAGACCGAACGUGAA GCGAGCACGCGUUCGGUCUGCUAACGUUCCGCAUCC
TS_Dr1s: 3WJ-L1'-L4-5bp-t4'	GGGACGGACAGCGUGCAUGGUGAAGCCUCCACGCCAUGCACGCUGCAGACCGAACGUGAA GCUCGCACGCGUUCGGUCUGCUAACGUUCCCCUGUC
TS_A2s: 3WJ-L1-L2'-4bp-t3	GGAAGGACAGCGUGCAUGGUGAAGGAGGCACGCCAUGCACGCUGCAGACCGAACGUGAAG UGGACACGCGUUCGGUCUGCUAACUUCCUCACCG
TS_Br2s: 3WJ-L3'-L2-4bp-t2	GGAAGGACAGCGUGCAUGGUGAAGCCUGCACGCCAUGCACGCUGCAGACCGAACGUGAAG UCCACACGCGUUCGGUCUGCUAACUUCCGGAUGC
TS_C2s: 3WJ-L3-L4'-4bp-t4	GGAAGGACAGCGUGCAUGGUGAAGCAGGCACGCCAUGCACGCUGCAGACCGAACGUGAAG CGAGCACGCGUUCGGUCUGCUAACUUCCGACAGG
TS_Dr2s: 3WJ-L1'-L4-4bp-t1	GGAAGGACAGCGUGCAUGGUGAAGCCUCCACGCCAUGCACGCUGCAGACCGAACGUGAAG CUCGCACGCGUUCGGUCUGCUAACUUCCCUCUGG
TS_B3s: 3WJ-L2-L3'-5bp-t3'	GGGACGGACAGCGUGCAUGGUGAAGUCCACACGCCAUGCACGCUGCAGACCGAACGUGAA GCCUGCACGCGUUCGGUCUGCUAACGUUCCCGGUGA
TS_D3s: 3WJ-L4-L1'-5bp-t4'	GGGACGGACAGCGUGCAUGGUGAAGCUCGCACGCCAUGCACGCUGCAGACCGAACGUGAA GCCUCCACGCGUUCGGUCUGCUAACGUUCCCCUGUC

TS_A4s: 3WJ-L1-L2'-9bp-t3	GGGAAGCACGGACAGCGUGCAUGGUGAAGGAGGCACGCCAUGCACGCUGCAGACCGAACG UGAAGUGGACACGCGUUCGGUCUGCUAACGUGUUUCCCUCACCG
TS_B4s: 3WJ-L2-L3'-9bp-t2	GGGAAGCACGGACAGCGUGCAUGGUGAAGUCCACACGCCAUGCACGCUGCAGACCGAACG UGAAGCCUGCACGCGUUCGGUCUGCUAACGUGUUUCCCGGAUGC
TS_C4s: 3WJ-L3-L4'-9bp-t4	GGGAAGCACGGACAGCGUGCAUGGUGAAGCAGGCACGCCAUGCACGCUGCAGACCGAACG UGAAGCGAGCACGCGUUCGGUCUGCUAACGUGUUUCCCGACAGG
TS_D4s: 3WJ-L4-L1'-9bp-t1	GGGAAGCACGGACAGCGUGCAUGGUGAAGCUCGCACGCCAUGCACGCUGCAGACCGAACG UGAAGCCUCCACGCGUUCGGUCUGCUAACGUGUUUCCCCUCUGG
TS_Ar6s: 3WJ-L2'-L1-9bp-t3	GGGAAGCACGGACAGCGUGCAUGGUGAAGUGGACACGCCAUGCACGCUGCAGACCGAACG UGAAGGAGGCACGCGUUCGGUCUGCUAACGUGUUUCCCUCACCG
TS_D8s: 3WJ-L4-L1'-9bp-t0	GGGAAGCACGGACAGCGUGCAUGGUGAAGCUCGCACGCCAUGCACGCUGCAGACCGAACG UGAAGCCUCCACGCGUUCGGUCUGCUAACGUGUUUCCCU
TTo constructs	
TTo_A1st: 3WJ-L1-L2'-5bp-t2	GGGACGGACAGCGUGCAUGGUGAAGGAGGCACGCCAUGCACGCUGCAGACCGAACGUGAA GUGGACACGCGUUCGGUCUGCUAACGUUCCGGAUGC
TTo_B1st: 3WJ-L2-L3'-5bp-t3	GGGACGGACAGCGUGCAUGGUGAAGUCCACACGCCAUGCACGCUGCAGACCGAACGUGAA GCCUGCACGCGUUCGGUCUGCUAACGUUCCUCACCG
TTo_T1st: 3WJ-L3-L1'-5bp-t4	GGGACGGACAGCGUGCAUGGUGAAGCAGGCACGCCAUGCACGCUGCAGACCGAACGUG AAGCCUCCACGCGUUCGGUCUGCUAACGUUCCGACAGG
TTo_A2st: 3WJ-L1-L2'-9bp-t3'	GGGAAGCACGGACAGCGUGCAUGGUGAAGGAGGCACGCCAUGCACGCUGCAGACCGAACG UGAAGUGGACACGCGUUCGGUCUGCUAACGUGUUUCCCCGGUGA
TTo_B2st: 3WJ-L2-L3'-9bp-t2'	GGGAAGCACGGACAGCGUGCAUGGUGAAGUCCACACGCCAUGCACGCUGCAGACCGAACG UGAAGCCUGCACGCGUUCGGUCUGCUAACGUGUUUCCCGCAUCC
TTo_T2st: 3WJ-L3-L1'-9bp-t4'	GGGAAGCACGGACAGCGUGCAUGGUGAAGCAGGCACGCCAUGCACGCUGCAGACCGAACG UGAAGCCUCCACGCGUUCGGUCUGCUAACGUGUUUCCCCCUGUC
TT constructs	
TT_A1t: 3WJ-L1-L2'-2bp-t2	GGGCUAACGCAGACCGAUGAAGGAGGCACGUCGGUCUGCGGACAGCCGUGCAUUGAAGUG GACACGAUGCACGGCUGCCCGGAUGC
TT_B1t: 3WJ-L2-L3'-2bp-t3	GGGCUAACGCAGACCGAUGAAGUCCACACGUCGGUCUGCGGACAGCCGUGCAUUGAAGCC UGCACGAUGCACGGCUGCCCUCACCG
TT_T1t: 3WJ-L3-L1'-2bp-t4	GGGCUAACGCAGACCGAUGAAGCAGGCACGUCGGUCUGCGGACAGCCGUGCAUUGAAGCC UCCACGAUGCACGGCUGCCCGACAGG
TT_A2t: 3WJ-L1-L2'-2bp-t4'	GGGCUAACGCAGACCGAUGAAGGAGGCACGUCGGUCUGCGGACAGCCGUGCAUUGAAGUG GACACGAUGCACGGCUGCCCCCUGUC
TT_B2t: 3WJ-L2-L3'-2bp-t3'	GGGCUAACGCAGACCGAUGAAGUCCACACGUCGGUCUGCGGACAGCCGUGCAUUGAAGCC UGCACGAUGCACGGCUGCCCCGGUGA
TT_T2t: 3WJ-L3-L1'-2bp-t2'	GGGCUAACGCAGACCGAUGAAGCAGGCACGUCGGUCUGCGGACAGCCGUGCAUUGAAGCC UCCACGAUGCACGGCUGCCCGCAUCC
TT_Tr3t: 3WJ-L1'-L3-6bp-t2'	GGGAUGGCUAACGCAGACCGAUGAAGCCUCCACGUCGGUCUGCGGACAGCCGUGCAUUGA AGCAGGCACGAUGCACGGCUGCCAUCCCGCAUCC
TT_B4t: 3WJ-L2-L3'-6bp-t3'	GGGAUGGCUAACGCAGACCGAUGAAGUCCACACGUCGGUCUGCGGACAGCCGUGCAUUGA AGCCUGCACGAUGCACGGCUGCCAUCCCCGGUGA
TT_Tr4t: 3WJ-L1'-L3-6bp-t4	GGGAUGGCUAACGCAGACCGAUGAAGCCUCCACGUCGGUCUGCGGACAGCCGUGCAUUGA AGCAGGCACGAUGCACGGCUGCCAUCCCGACAGG
TT_A5t: 3WJ-L1-L2'-2bp-t5'	GGGCUAACGCAGACCGAUGAAGGAGGCACGUCGGUCUGCGGACAGCCGUGCAUUGAAGUG GACACGAUGCACGGCUGCCCGGUGUC
TT_B5t: 3WJ-L2-L3'-2bp-t4'	GGGCUAACGCAGACCGAUGAAGUCCACACGUCGGUCUGCGGACAGCCGUGCAUUGAAGCC UGCACGAUGCACGGCUGCCCCCUGUC
TT_Tr5t: 3WJ-L1'-L3-6bp-t3	GGGAUGGCUAACGCAGACCGAUGAAGCCUCCACGUCGGUCUGCGGACAGCCGUGCAUUGA AGCAGGCACGAUGCACGGCUGCCAUCCCUCACCG
TT_Tr6t: 3WJ-L1'-L3-6bp-t2	GGGAUGGCUAACGCAGACCGAUGAAGCCUCCACGUCGGUCUGCGGACAGCCGUGCAUUGA AGCAGGCACGAUGCACGGCUGCCAUCCCGGAUGC
TT_Ar7t: 3WJ-L2'-L1-2bp-t5	GGGCUAACGCAGACCGAUGAAGUGGACACGUCGGUCUGCGGACAGCCGUGCAUUGAAGGA GGCACGAUGCACGGCUGCCCGACACC
TT_B7t: 3WJ-L2-L3'-2bp-t2'	GGGCUAACGCAGACCGAUGAAGUCCACACGUCGGUCUGCGGACAGCCGUGCAUUGAAGCC UGCACGAUGCACGGCUGCCCGCAUCC

B. RNA composition of 3WJ-nanostructures

Nanostructures	Building blocks
TectoSquare TS	**TS** (TS-A0s, TS-B0s, TS-C0s, TS-D0s)
TectoTriangle TTo	**TTo** (TS-A0s, TS-B0s, TTo-T0st)
TectoTriangle TT	**TT** (TT-A0t, TT-B0t, TT-T0t)
TectoSquare TSa	**TSa** (TT-A0t, TT-B0t, TSa-C0ts, TSa-D0ts)
3WJ_TS-Brick-Array	**TS1** (TS-A1s, TS-Br1s, TS-C1s, TS-Dr1s) **+ TS2** (TS-A2s, TS-Br2s, TS-C2s, TS-Dr2s)
3WJ_TS-Plaid_Array	**TS3** (TS-A1s, TS-B3s, TS-C1s, TS-D3s) **+ TS4** (TS-A4s, TS-B4s, TS-C4s, TS-D4s)
3WJ_TS-2x2-Ladder	**TS5** (TS-A1s, TS-Br1s, TS-C1s, TS-D3s) **+ TS6** (TS-Ar6s, TS-B4s, TS-C4s, TS-D4s)
3WJ_TS-2x2_Grid	**TS7** (TS-A0s, TS-Br1s, TS-C1s, TS-D3s) **+ TS8** (TS-Ar6s, TS-B4s, TS-C4s, TS-D8s)
3WJ_TTo-Honeycomb_Mix	**TTo1** (TTo-A1st, TTo-B1st, TTo-T1st) **+ TTo2** (TTo-A2st, TTo-B2st, TTo-T2st)
3WJ_TT-Triangle-Array	**TT1** (TT-A1t, TT-B1t, TT-T1t) **+ TT2** (TT-A2t, TT-B2t, TT-T2t)
3WJ_TT-Diamond-Ladder	**TT3** (TT-A1t, TT-B1t, TT-Tr3t) **+ TT4** (TT-A2t, TT-B4t, TT-Tr4t)
3WJ_TT-3T_Grid	**TT5** (TT-A5t, TT-B5t, TT-Tr5t) **+ TT6** (TT-A0t, TT-B2t, TT-Tr6t) **+ TT7** (TT-Ar7t, TT-B7t, TT-Tr4t)

C. TectoRNA sequences to build tectofibers and AMP-responsive nanorings

TectoRNA nomenclature: TF stands for tectoRNA forming fibers and nanorings. Two TF units (A and B) assemble through complementary KL interactions (Loop L1 with L1' and loop L2 with L2' to form nanostructures[11]. TF are based on the A-minor junction (AmJ), which can either involve a helix/GAAA interaction or 11nt/GAAA interaction. AmJ-AMP stands for TF units incorporating an AMP aptamer. Yellow indicates the position of KLs. Blue and green indicate nucleotide positions for RNA tertiary modules. Grey indicates mutated positions within the AmJ and AMP aptamer modules.

TectoRNAs	Sequences
A-minor Tectofibers	
TF1_A: AmJ-Helix_GAAA_A L1-L2'	GGAUGGGAAACGUGGUCCGAUCUGAAGGAGGCACGGAUUGGACUACGCCAAGUCGAU GAAGUGGACACGUCGAUUUGGUCAUUCUU
TF1_B: AmJ-Helix_GAAA_B L2-L1'	GGAUGGGAAACGUGGUCCGAUCUGAAGUCCACACGGAUUGGACUACGCCAAGUCGAU GAAGCCUCCACGUCGAUUUGGUCAUUCUU
TF2_A: AmJ-11nt_GAAA_A L1-L2'	GGAUGGGAAACGUGGUCCGAUCUGAAGGAGGCACGGAUUGGACUACGCUAAGUCGAU GAAGUGGACACGUCGAUAUGUCAUUCUU
TF2_B: AmJ-11nt_GAAA_B L2-L1'	GGAUGGGAAACGUGGUCCGAUCUGAAGUCCACACGGAUUGGACUACGCUAAGUCGAU GAAGCCUCCACGUCGAUAUGUCAUUCUU
AMP A-minor tectofibers and nanorings	
AMP-TF1_M: AmJ-AMP_M L1-L1'	GGGUACAGGGAAACGUCGGGGAAGAAACUGCGCAUGUGAAGGAGGCACGCAUGCGGC CGACGCGGGAGUCGUGAAGCCUCCACGCGACUCCCGUCUGUAUCUU
AMP-TF1_A: AmJ-AMP_A L1-L2'	GGGUACAGGGAAACGUCGGGGAAGAAACUGCGCAUGUGAAGGAGGCACGCAUGCGGC CGACGCGGGAGUCGUGAAGUGGACACGCGACUCCCGUCUGUAUCUU
AMP-TF1_B: AmJ-AMP_B L2-L1'	GGGUACAGGGAAACGUCGGGGAAGAAACUGCGCAUGUGAAGUCCACACGCAUGCGGC CGACGCGGGAGUCGUGAAGCCUCCACGCGACUCCCGUCUGUAUCUU
AMP-TF1m1_A: AmJ_m-AMP_A L1-L2'	GGGUACAGGGAAUCGUCGGGGAAGAAACUGCGCAUGUGAAGGAGGCACGCAUGCGGC CGACGCGGGAGUCGUGAAGUGGACACGCGACUCCCGUCUGUAUCUU
AMP-TF1m1_B: AmJ_m-AMP_B L2-L1'	GGGUACAGGGAAUCGUCGGGGAAGAAACUGCGCAUGUGAAGUCCACACGCAUGCGGC CGACGCGGGAGUCGUGAAGCCUCCACGCGACUCCCGUCUGUAUCUU
AMP-TF1m2_A: AmJ-AMP_m_A L1-L2'	GGGUACAGGGAAACGUCGGGCAAGAAACUGCGCAUGUGAAGGAGGCACGCAUGCGGC CGACGCGGGAGUCGUGAAGUGGACACGCGACUCCCGUCUGUAUCUU
AMP-TF1m2_B: AmJ-AMP_m_B L2-L1'	GGGUACAGGGAAACGUCGGGCAAGAAACUGCGCAUGUGAAGUCCACACGCAUGCGGC CGACGCGGGAGUCGUGAAGCCUCCACGCGACUCCCGUCUGUAUCUU
AMP-TF1m3_A: AmJ_m-AMP_m_A L1-L2'	GGGUACAGGGAAUCGUCGGGCAAGAAACUGCGCAUGUGAAGGAGGCACGCAUGCGGC CGACGCGGGAGUCGUGAAGUGGACACGCGACUCCCGUCUGUAUCUU

AMP-TF1m3_B: AmJ_m-AMP_m_B L2-L1′	GGGUACAGGGAAUCGUCGGGCAAGAAACUGCGCAUGUGAAGUCCACACGCAUGCGGC CGACGCGGGAGUCGUGAAGCCUCCACGCGACUCCCGUCUGUAUCUU
AMP-TF2_A: AmJ-AMP_A_r L1-L2′	GGAUGGGAAACGUGGCGGCGCAUGAAGGAGGCACGUGCGGGAAGAAACUGCGCCACG CCAAGUCGAUGAAGUGGACACGUCGAUUUGGUCAUUCUU
AMP-TF2_B: AmJ-AMP_B_r L2-L1′	GGAUGGGAAACGUGGCGGCGCAUGAAGUCCACACGUGCGGGAAGAAACUGCGCCACG CCAAGUCGAUGAAGCCUCCACGUCGAUUUGGUCAUUCUU
AMP-TF2m_A: AmJ-AMP_m_A_r L1-L2′	GGAUGGGAAACGUGGCGGCGCAUGAAGGAGGCACGUGCGGCAAGAAACUGCGCCACG CCAAGUCGAUGAAGUGGACACGUCGAUUUGGUCAUUCUU
AMP-TF2m_B: AmJ-AMP_m_B_r L2-L1′	GGAUGGGAAACGUGGCGGCGCAUGAAGUCCACACGUGCGGCAAGAAACUGCGCCACG CCAAGUCGAUGAAGCCUCCACGUCGAUUUGGUCAUUCUU

D. TectoRNA sequences to build "heart" shaped nanostructures

TectoRNA nomenclature: sequence units entering into the composition of G1 and G2 nano-hearts are also represented Fig. 1 and S7. Blue and green indicate the nucleotide positions of RNA tertiary modules. Yellow indicates the position of KLs. Grey indicates positions involved in the formation of tail-tail or triple helix tail-tail interactions.

	TectoRNAs	Sequences
	G1 nano-heart	
G1-heart units	**HW:** tRNA-L3-L3 (162nt)	GGGACCUCCGUGGUUCGAAUCCACGUACUAGCCUGGAUGAAUUCCCAGUGAAGCAGGCACGCUG GGAGUUCGUCCAGGCUGGUAUGGCCGAGCGGCUGAAGGCACUCCGACGCGGUCUGCGCUGAAGC AGGCACGGCGUAGGCCGCGUUGGAGUAGGUCCCU
	HX: AmJ-Ab-L2-L3′ (130nt)	GGGACAGGGAAACGUGAGACCGUUGGCUUGGCAAUUGUGAAGUCCACACGCAAUUAGCCAAGCU AACGGUCUCACGCCGAUCCUUGAGGUCGUGAAGCCUGCACGCGAUCUCAAGGAUCGGUCUGUCC UU
	HY: AmJ-AMP-L2′-L1′ (120nt)	GGGGAGGGAAACGUGGCGGCUUGGCUGAAUGAAGUGGACACGUUCAGCCAAGGGAAGAAACUGC GCCACGCCGAGGGAAGAAACUGCGACGUGAAGCCUCCACGCGUCGGCUCGGUCUCCCCU
	HZ: tRNA-L1-L1 (123nt)	GGGACCUCCGUGGUUCGAAUCCACGUACUAGCCUGGAUGAAGGAGGCACGUCCAGGCUGGUAUG GCCGAGCGGCUGAAGGCACUUCAACGUGAAGGAGGCACGCGUUGGAGUAGGUCCCU
	G2 nano-heart	
G2-heart units	**HA1:** 3WJ-L3-L7 (91nt)	GGGAAUUCCUAACAGACCGACGUGAAGCAGGCACGCGUUGGUCUGGACAGCGGUAUGGUGAACG UGGUACGCCAUGCCGCUGGAGUUCCCU
	HA2: 3WJ-L7-L3 (91nt)	GGGAAUUCCUAACAGACCGACGUGAACGUGGUACGCGUUGGUCUGGACAGCGGUAUGGUGAAGC AGGCACGCCAUGCCGCUGGAGUUCCCU
	HB: 3WJ_Ab-L3′-L5′-t (145nt)	GGGAAUUCGACGUCGCUGCAGUUCCUGGACCACGUGAAGCCUGCACGCGUGGUUCAGGGACUGC UAACAGAUCAUCGUACGCAACGGUGAAGAACGCACGCCGUUAGCGUGCGAUGGUCUGGACAGCG GCGUCGAGCCAAGGUGU
	HC: AmJ_AMP-L5-L1′ (123nt)	GGGGAGGGAAACGUGGCGGCUUGGCUGAAUGAAGCGUUCACGUUCAGCCAAGGGAAGAAACUGC GCCACGCCGAGGGAAGAAACUGCGACGUGAAGCCUCCACGCGUCGGCUCGGUCUCCCCU
	HD: 3WJ-L1-L4-t′ (104nt)	GGGAAUUCGAGGACUGGUCUGGACAGCGACUGAAGGAGGCACGGUCGCUGCAGGCAUGAAGCUC GCACGUGCUUGCUAACAGAUCAGUUCUCGAGCCUUGGUGU
	HE: AmJ_AMP-L6′-L4′ (123nt)	GGGGAGGGAAACGUGGCGGCUUGGCUGAAUGAAGGUGACACGUUCAGCCAAGGGAAGAAACUGC GCCACGCCGAGGGAAGAAACUGCGACGUGAAGCGAGCACGCGUCGGCUCGGUCUCCCCU
	HF: AmJ_11nt_Ab-L6-L7′ (125nt)	GGAAGGGAAACGUACCGGAUCAACGUACGCAACGGUGAAGUCACCACGCCGUUAGCGUGCGUUG GUCUGGUACGCUAAGCUGAGACCACGUGAGACCACGACGCGUGGUUUCAGUAUGUCUUCUU
	nano-heart dimers	
Dimer units	**HA1_t1:** 3WJ-L3-L7-t1	GGGAAUUCCUAACAGACCGACGUGAAGCAGGCACGCGUUGGUCUGGACAGCGGUAUGGUGAACG UGGUACGCCAUGCCGCUGGAGUUCCCCCAGAGC
	HA1_t1′: 3WJ-L3-L7-t1′	GGGAAUUCCUAACAGACCGACGUGAAGCAGGCACGCGUUGGUCUGGACAGCGGUAUGGUGAACG UGGUACGCCAUGCCGCUGGAGUUCCCGCUCUGG
	HA2_t1: 3WJ-L7-L3-t1	GGGAAUUCCUAACAGACCGACGUGAACGUGGUACGCGUUGGUCUGGACAGCGGUAUGGUGAAGC AGGCACGCCAUGCCGCUGGAGUUCCCCCAGAGC
	HA2_t1′: 3WJ-L7-L3-t1′	GGGAAUUCCUAACAGACCGACGUGAACGUGGUACGCGUUGGUCUGGACAGCGGUAUGGUGAAGC AGGCACGCCAUGCCGCUGGAGUUCCCGCUCUGG

E. G3-heart sequence

Nomenclature: Parentheses indicate positions involved in the secondary structure. Brackets indicate positions involved in kissing loop (KL) complexes. Tertiary module sequences: UA_h_3WJ are in blue; KLs are in yellow; AMP aptamers are in green; A-minor junctions are in grey; UNCG tetraloops are in red; A-bulges are in magenta. See also Figure S8.

Heart G3A (A1_KL1-6)

```
((((((((...((((((((((((((((((((((((((((((((((((((((...((((((((((((((((((((((((((((((((((((((((
GGAACGCCUAACCGUGCAGGAGCGCAGAGGGUGAUCGGUUGUAGCGUGGUCUAACUGCGUUUCGUUUUCAAACAGUAAAUGCAGCGCCACACG
(((...........((((((((((((...........(((((((..[[[[[[.))))))).))))))))(((((((....))))))))(....)
GUGGGAAGAAACUGCUUAGCGCCCAGGGAAGAAACUGCCUCGUGAAGCCUCCACGCGAGGGCUGGGUCGUUUGUAUUCGUACGAACGGGUAAC
)))))).)))))))))))))))))))))))))).))))))))))))))))...(((((((((((((((((((((((((((((((((((...((
GCUGAGGCACUGUGUGGUGCUGCGUUUAUUGUUUAGAAGACGAAAUGCAGGACAGUCAGCAUCCGAUCUAUUCAAUAGGGGAUCUGAGGACAG
((((((..]]]]]].))))))))((((((((((((((((((((((((.((((((((((((((....))))))))(....)(((((((.((((((
AAAAUGAAGGAGGCACGUUUUCUGGGCUCGGACGUGGCCCGUCGACGGCCUGGUCGGUGUCAUUCGUGACAUCGGGUAACGUUAAGGCCAUGC
((((((..[[[[[[.))))))))))))...........))))))))))))...........))))))))))))))))))))))))...)))
AUUAUUGAAGGUGACACGAUAGUGCGUGGGGAAGAAACUGCUUAACGCCAGGGGAAGAAACUGCGUUGACGGGUCACGUUCGGGCCCUAACUC
)))))))))))))))))))))))))))))))))))))))))))))))))))))))))))))))))))))))...(((((((((((((((((
GGAUCCCUUAUUGGAUAGAUUGGAUGUUGACUGACUACGCUAUAACCGGUCACCUUCUGCGUUCCUGUACGGGACAGCGUUGGGCGGAAAUG
(((((((((((((((((((..((((((((((....))))))))(....)(((((((((((((((((((((((((((..]]]]]].)))))).))))
UCUACUCCGUUCUGUUGUAUGUCACGCGAUUCGUCGUGUGGGAAACGUUGGUGGGAGAGUGGCACAUGGAUGAAGUCACCACGUCCAUAGUGC
)))))))))))))))))...))))))))))))))))))))))))))))))))))))))))))))
UACUCUUCCACCGACGCUAAGCAACGGAACGGGGUAGAUAUUUCUGCCCCAGCGCUGGUGUUUC
```

3. Supplementary Figures

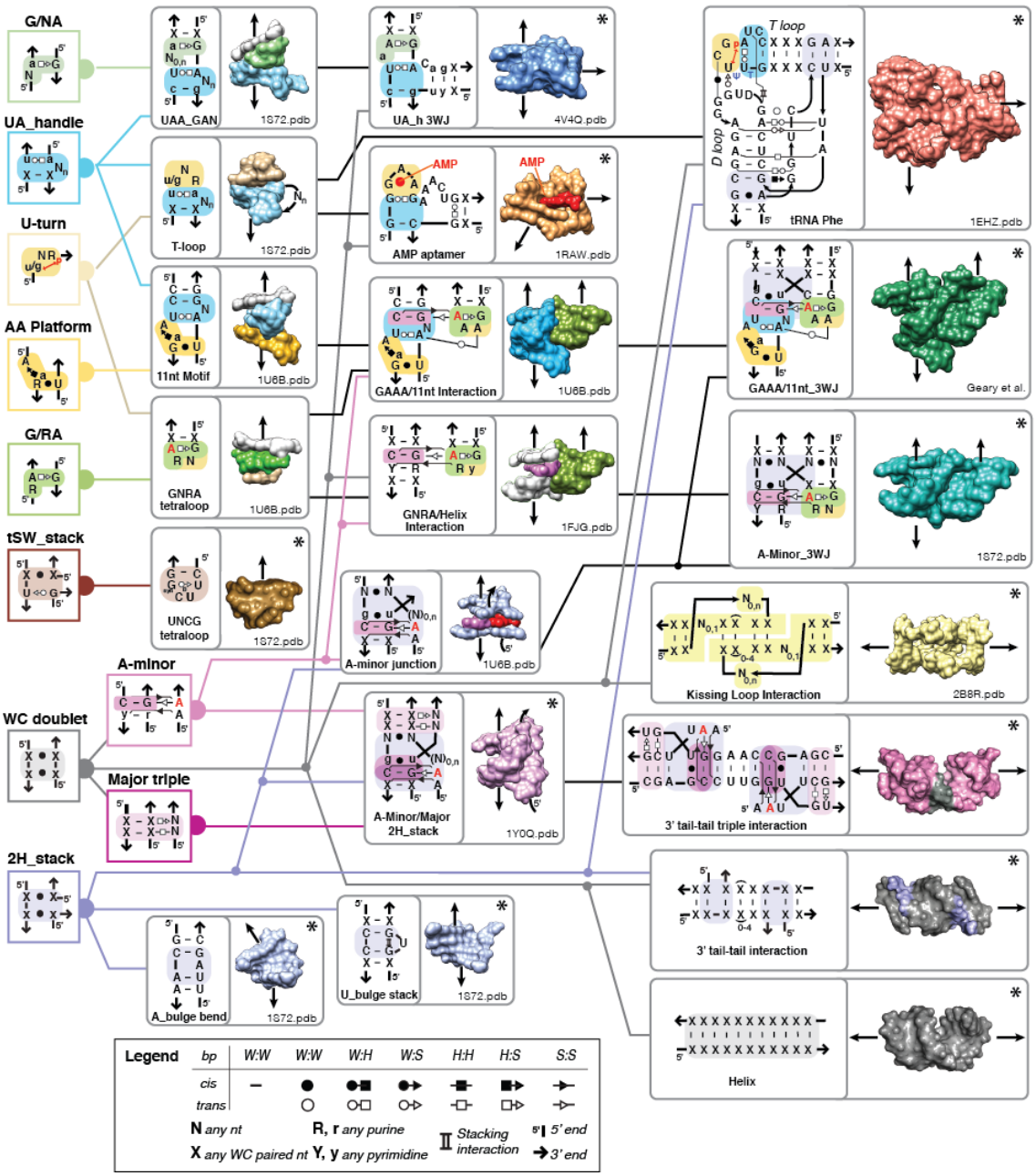

Figure S1: Syntax of RNA structural modules used for nano-construction. An RNA structural module is defined by a set of conserved and semi-conserved nucleotides that specifies for canonical and non-canonical base pairs and other three-dimensional interactions. Base pairs involve either the Watson-Crick (W), Hoogsteen (H), shallow groove (S) edges of a nucleotide (see boxed legend). The resulting nucleotide network codes for a particular conformational 3D space or set of preferential RNA conformers. The complexity of the structural 3D modules is shown increasing from the left to the right. Asterisks indicate RNA modules used as structural building blocks in this study. The nomenclature[12] of interactions takes advantage of the syntax of RNA modules previously described in references[11, 13, 14]. The 3D structure on the right of each module pattern is extracted from X-ray structures available in the Protein Data Bank: E.coli 23S rRNA (PDB_ID:4V4Q); Twort (PDB_ID: 1Y0Q) and Azoarcus (PDB_ID: 1U6B) group I introns; H.marismortui 23S rRNA (PDB_ID: 1S72); Yeast tRNA-Phe (PDB_ID: 1EHZ); HIV-1 DIS (PDB_ID: 2B8R); AMP aptamer conformer 1 (PDB_ID: 1RAW). The color code of each module used for nano-construction is the same as for Figures 1 and S2.

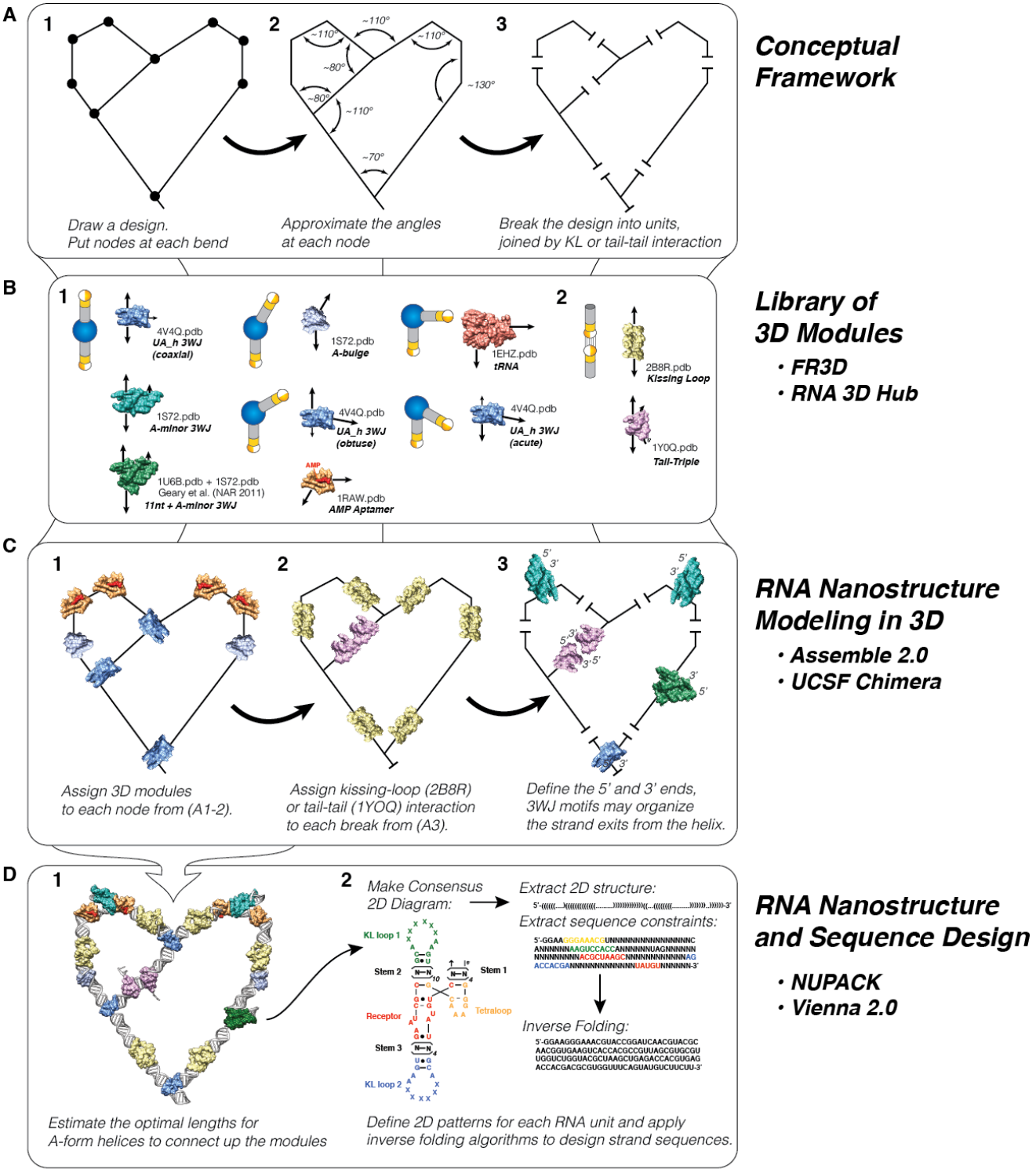

Figure S2: Process of design and nano-construction of RNA self-assembling architectures. (**A**) Design of the conceptual framework aiming at taking advantage of a specific set of structural constraints. (**B**) Set of RNA modules specifying for specific structural constraints. (**C**) Rational modeling in 3D of the RNA nanostructures. (**D**) Design of the RNA sequence aimed at folding into a unique 2D structure through minimization of alternative folds. See text from the extended Materials and Methods section for explanation.

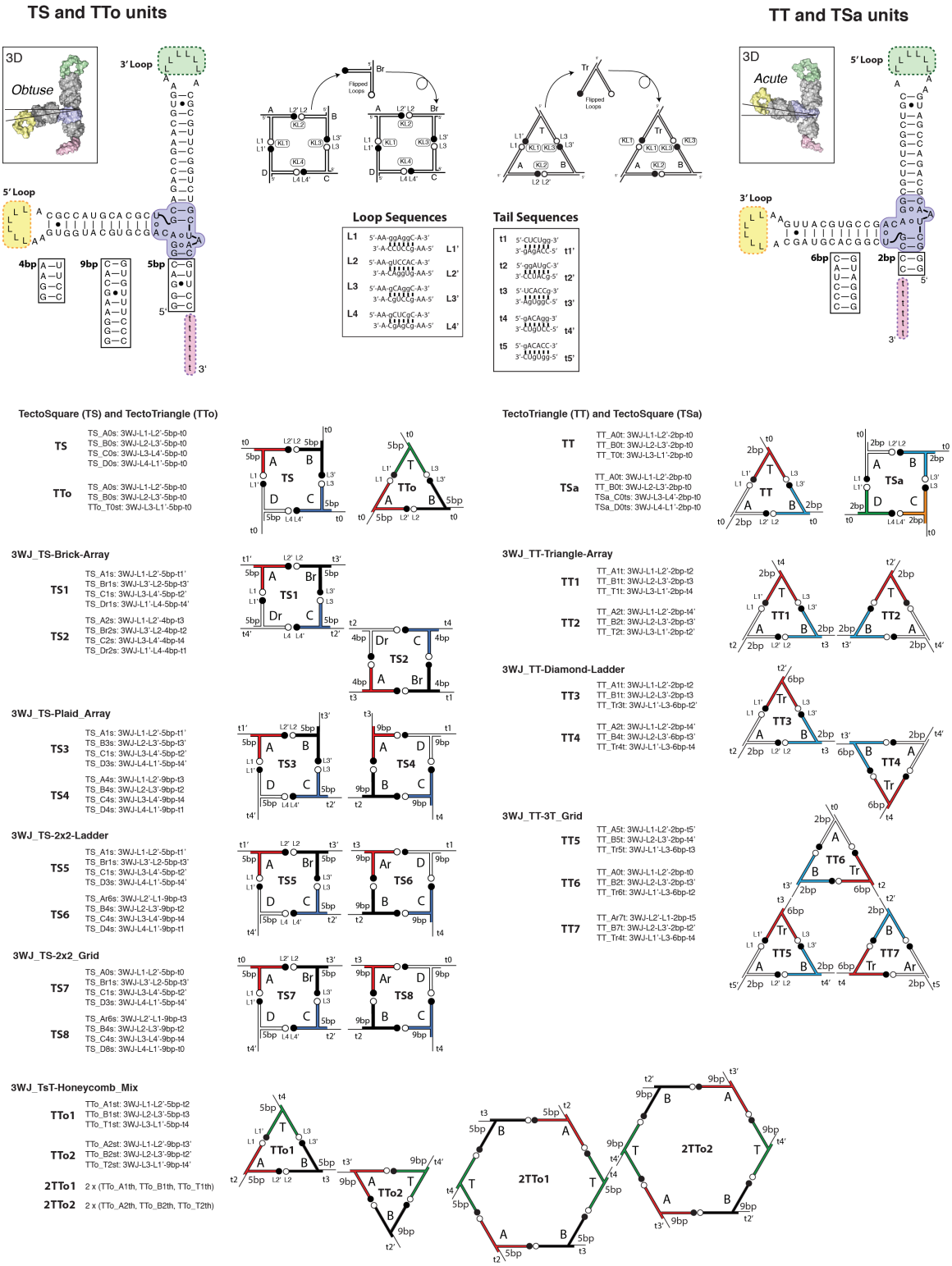

Figure S3: Diagram describing the sequence of molecules used for preparing UAh-3WJ tectosquare and tectotriangle assemblies. The 2D diagrams are shown on the top left and right. TS stands for tectosquare, TT stands for tectotriangle. Tectotriangle TTo is made of obtuse units designed for tectosquare. Tectosquare TSa is made of acute units designed for tectotriangle. The different nanostructure patterns and their assembly rules are indicated. Different sequences of connecting stems are used (either 4bp, 5bp or 9bp for TS units and 2bp or 6bp for TT units), with a 3' tail appended for making tail-tail connections. 3WJ units are programmed *via* different combinations of KLs, connecting stems and tails. Different combinations of TS and TT assemble in 15 mM Mg^{2+} buffer into different arrays.

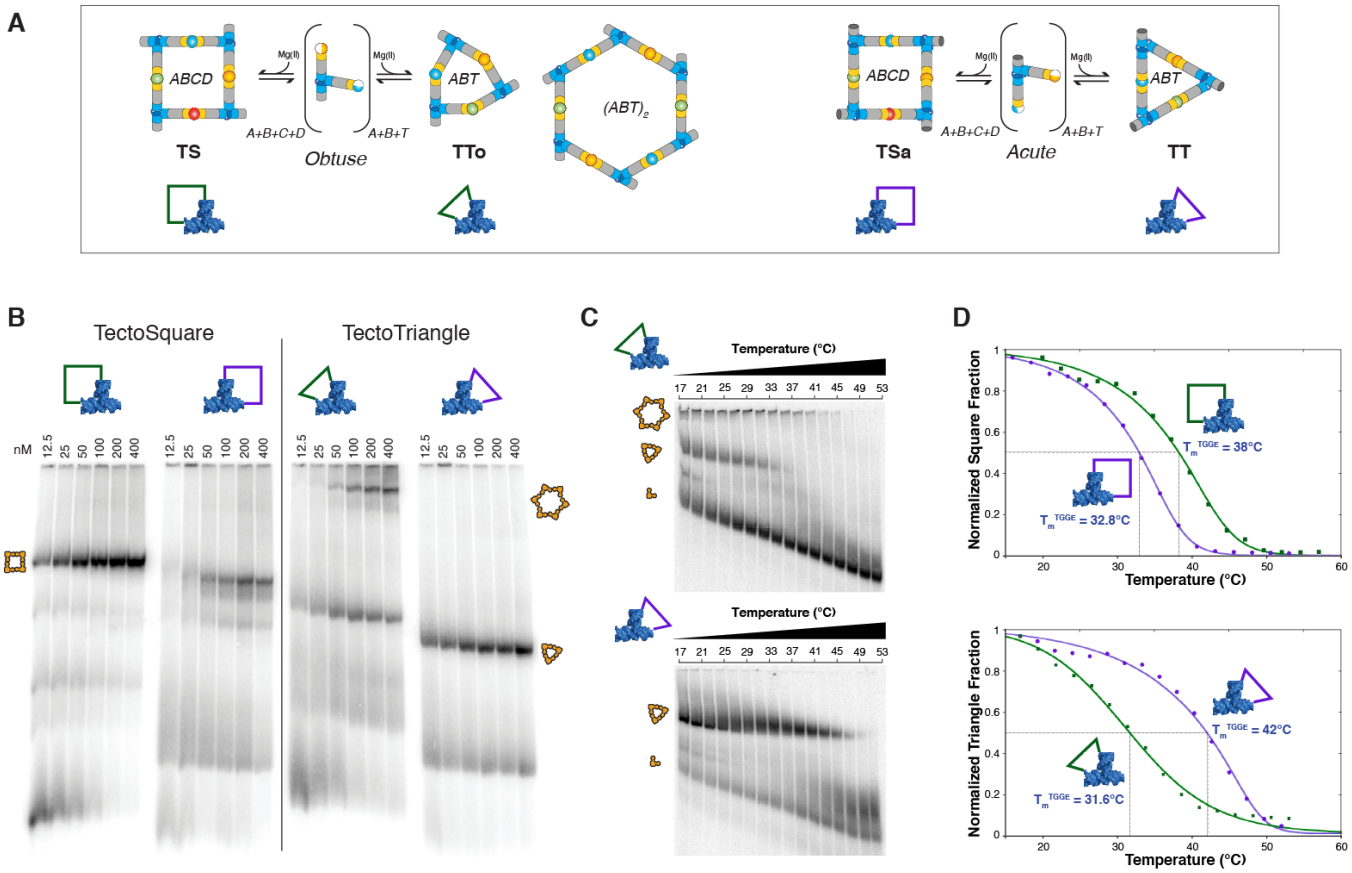

Figure S4: Characterizations of UAh-3WJ tectosquares (TS and TSa) and tectotriangles (TT and TTo) by native polyacrylamide gel electrophoresis (native PAGE) and temperature gradient gel electrophoresis (TGGE) (see also Materials and Methods). These nanostructures are based on the UAh_3WJ module. (**A**) TS and TTo nanostructures are generated with "obtuse" units favoring TS versus TT. TSa and TT are generated with "acute" units favoring TT versus TS. (**B**) The 7% Native PAGE analysis were performed after RNA assembly in presence of 15 mM $Mg(OAC)_2$, 50 nM KCl and TB buffer at 10°C. (**C**) TGGE gels for TTo and TT tectotriangles assembled at 0.2 mM $Mg(OAc)_2$, 50mM KCl, TB buffer. RNA concentration was 50 nM. (**D**) Plots of the disassembly melting profiles for TS, TSa, TTo and TT nanostructures and their apparent melting temperatures (Tm) obtained at 0.2 mM $Mg(OAc)_2$ from analysis of TGGE experiments as shown in (c). TGGE Tms are 31.6°C, 32.8°C, 38°C and 42°C for TTo, TSa, TS and TT, respectively. TGGE Tm for 2TTo (Hexamer of TTo units) is ~37°C (not shown).

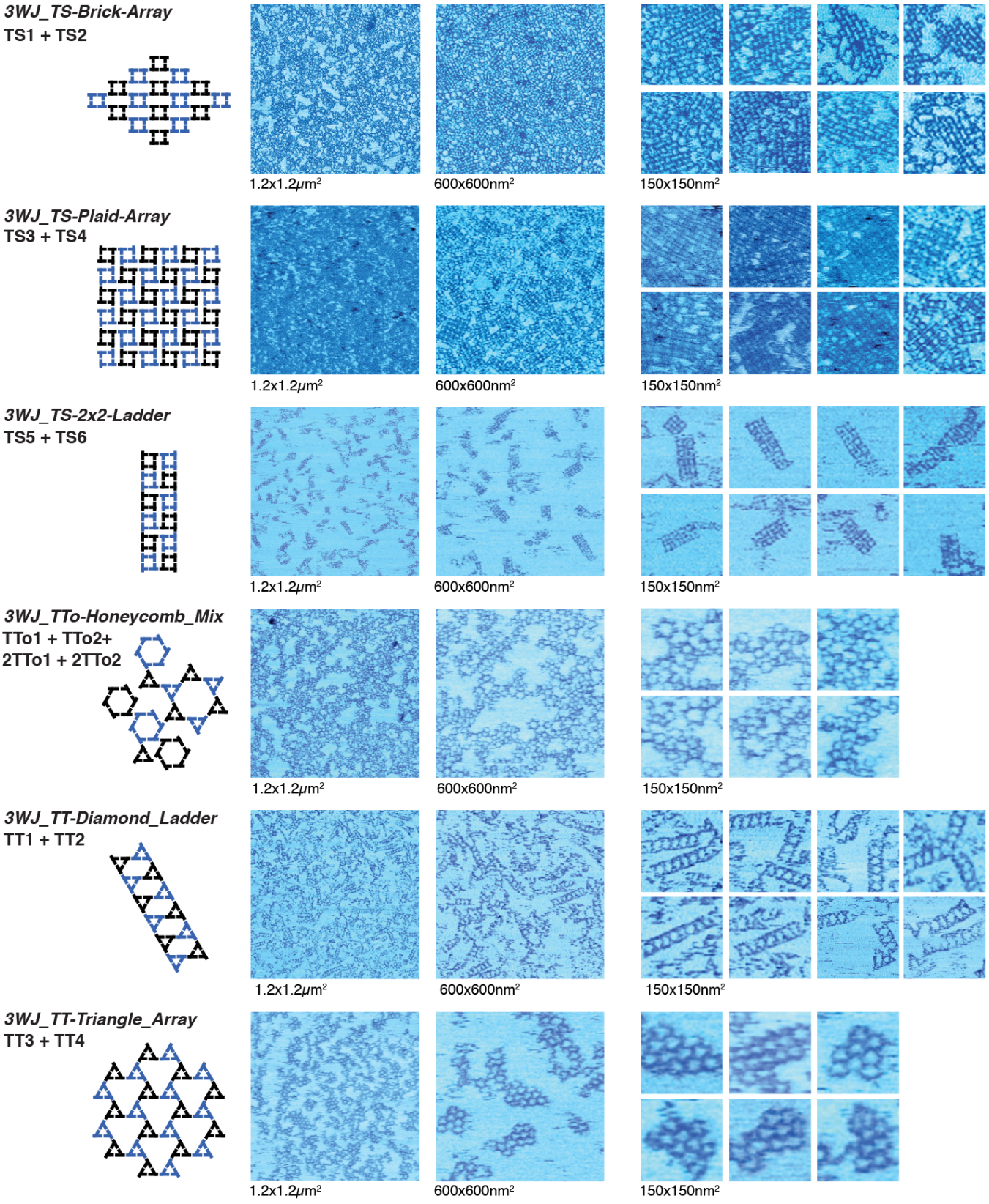

Figure S5A: (see legend next page)

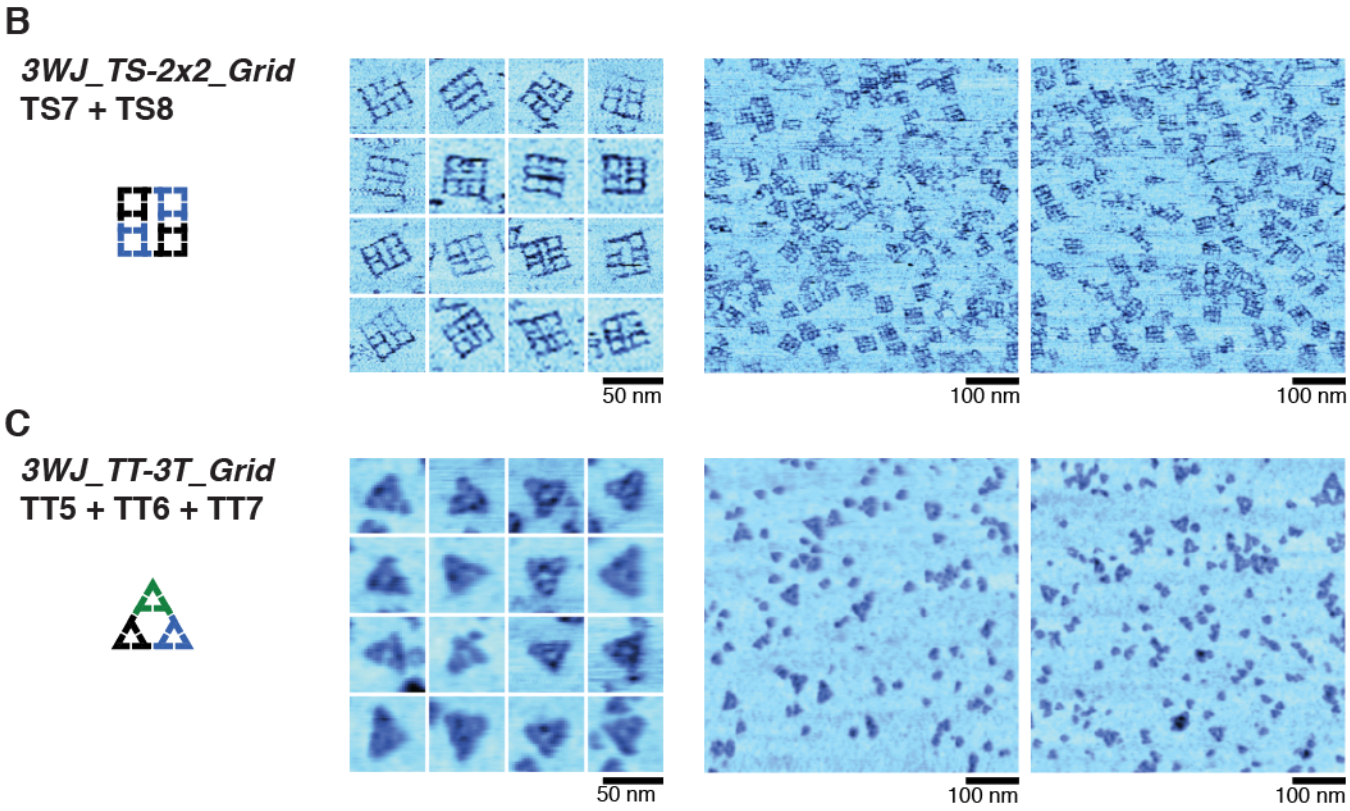

Figure S5: High-resolution AFM images of various RNA nanostructures built from tectosquares (TS) and tectotriangles (TT and TTo) with the UAh_3WJ module. (**A**) Array compositions in TS and TT are corresponding to those depicted in Figure S3. AFM images were acquired under solution with 15mM $Mg(OAc)_2$, TB buffer as described in the Material and Methods. For the 3WJ_TTo-honeycomb mix, TTo triangle units form a heterogeneous mixture of triangles and hexagons (2TTo), which self-assemble into an irregular RNA fabric of triangles and small and large hexagons. (**B,C**) AFM images of TS and TT programmable nano-grids. (**B**) TS 2x2 nanogrids were imaged under solution. (**C**) TT nanogrids were imaged in air as described in Material and Methods.

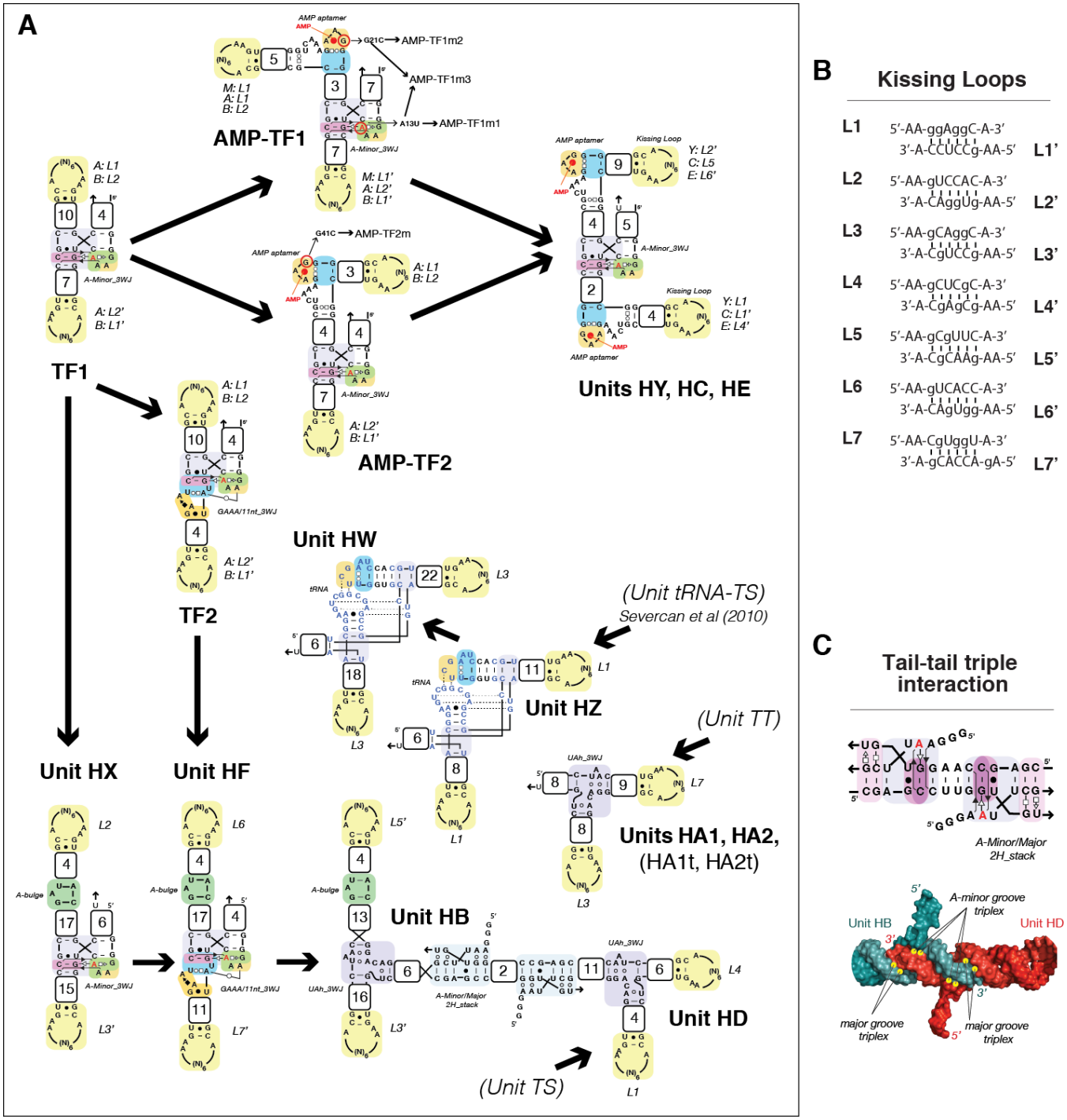

Figure S6: Secondary structure diagrams and assembly rules for TF, AMP-TF and G1 and G2 nano-heart units. (**A**) Structural relationships between the various units entering into the composition of TF nanofibers, nanorings, and heart-shaped nanostructures are indicated by black arrows. The structural modularity is highlighted as indicated in Figure S1. Unit HZ is based on the unit entering into the composition of tRNA squares and polyhedrons[1,2]. Units HA1, HA2 and Unit HD are based on 3WJ-RNA units entering into the composition of TS and TT building blocks, respectively. While structurally different, unit HF and unit HB are topologically equivalent. Point mutations within AMP-TF1 and AMP-TF2 units are circled in red (see also Table S1). The type of kissing loops (L1 to L7 and L1' to L7') is indicated for the different units. (**B**) Kissing loops (KL) used in these nanostructures. (**C**) Detail of the tail-tail interaction between units HB and HD.

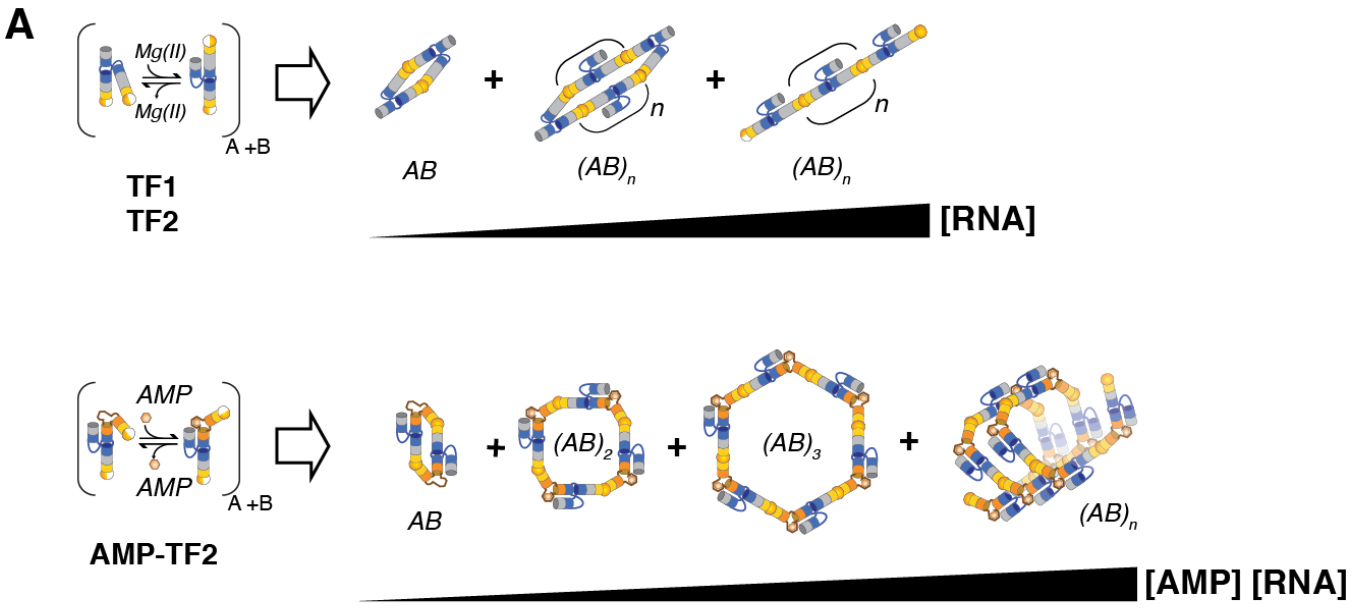

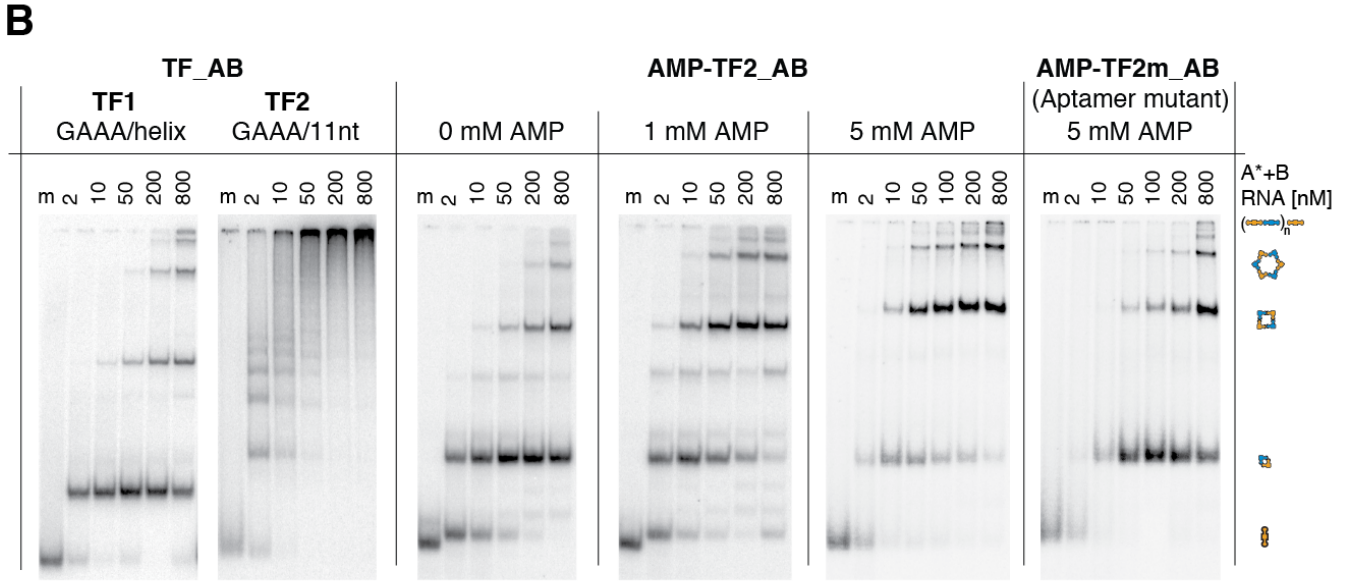

Figure S7(AB): Self-assembly of RNA nanofibers and nanorings based on the A-minor junction and AMP aptamer modules. (**A**) Schematic of the different nanostructures resulting from self-assembly of TF1, TF2 and AMP-TF2 bi-molecular unit systems (units A and B). Higher is the RNA concentration and/or AMP concentration, larger molecular weight nanostructures are produced. (**B**) Native PAGE showing the end-to-end self-assembly of TF1, TF2 and AMP-TF2 at various equimolar concentrations of A and B units in presence of 1mM $Mg(OAc)_2$, 10 mM TB pH 8.2, 50 mM KCl at 10°C. Self-assembly of AMP-TF2 units were tested in absence or presence of AMP at the indicated concentration. The mutant aptamer units are AMP-TF2 units with a point mutation (G41 to C), which prevents binding of AMP. For each type of constructs, experiment includes one lane (lane m) loaded with only unit A, as a molecular control. Long molecular fibers are trapped on the top of the gel.

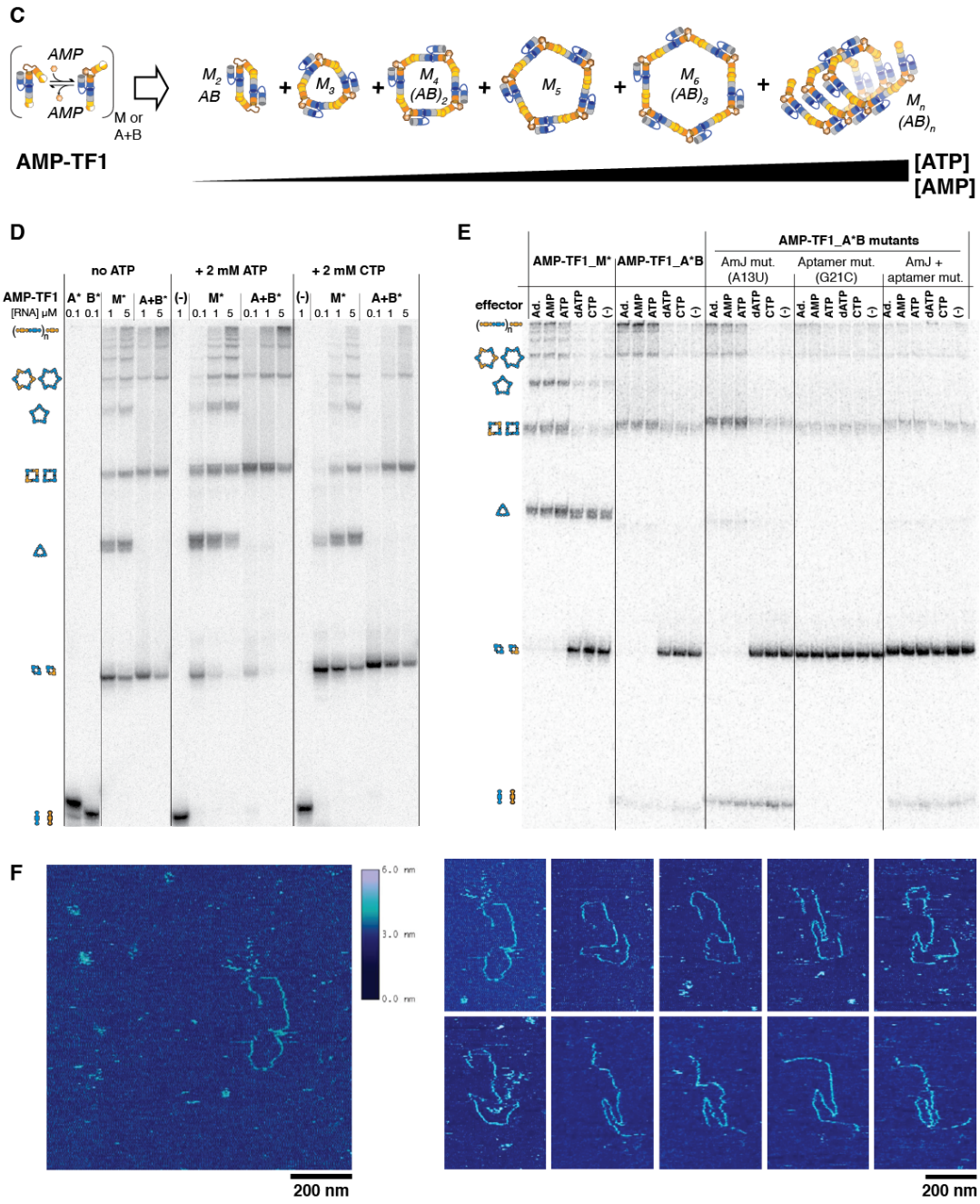

Figure S7(C-F): AMP dependent self-assembly of RNA nanofibers. (**C**) Schematic of the different nanostructures resulting from self-assembly of AMP-TF1 units at various RNA concentrations in presence or absence of ATP (or AMP). Monomeric unit M self-assembles into nanostructures with an even and odd number of units while bimolecular units A and B form assemblies with even number of units only. (**D**) AMP-TF1 units assembled at 15°C without or with 2 mM of ATP (or CTP) in presence of 2 mM $Mg(OAc)_2$, 50 mM KCl, 10 mM TB (pH 8.2), for 45 min before separation on 7% native PAGE (0.2mM $Mg(OAc)_2$, 50 mM KCl, 10 mM TB (pH 8.2)). (**E**) Efficient assembly of AMP-TF1 units into high molecular weight nanostructures is specific to the adenosine moiety of AMP and ATP. Units with the AMP aptamer mutation (G21-C) do not assemble into large nanostructures in presence of adenosine, AMP or ATP. Mutation (A13-U) in the A minor junction module does not affect self-assembly in the conditions tested. AMP-TF1 units [1 µM] were assembled without or with 1.5 mM (Adenosine (Ad.), AMP, ATP, dATP, CTP) in 2mM $Mg(OAc)_2$, 50 mM KCl, 10 mM TB (pH 8.2)) at 30°C for 90 min before separation on 8% native PAGE (0.2 mM $Mg(OAc)_2$, 50 mM KCl, 10 mM TB (pH 8.2)). For (D,E), self-assembly experiment with units A and B were performed at equimolar concentration. Radiolabeled units are indicated by asterisk. (**F**) AFM images of AMP-TF1 nanofibers (25 nM) were acquired in presence of 2 mM ATP under solution (15 mM $Mg(OAc)_2$, TB buffer) at 20°C as described in the Material and Methods. These RNA fibers present kinks suggesting that AMP-TF1 assemble into spiral fibers that do not stick well to the mica surface.

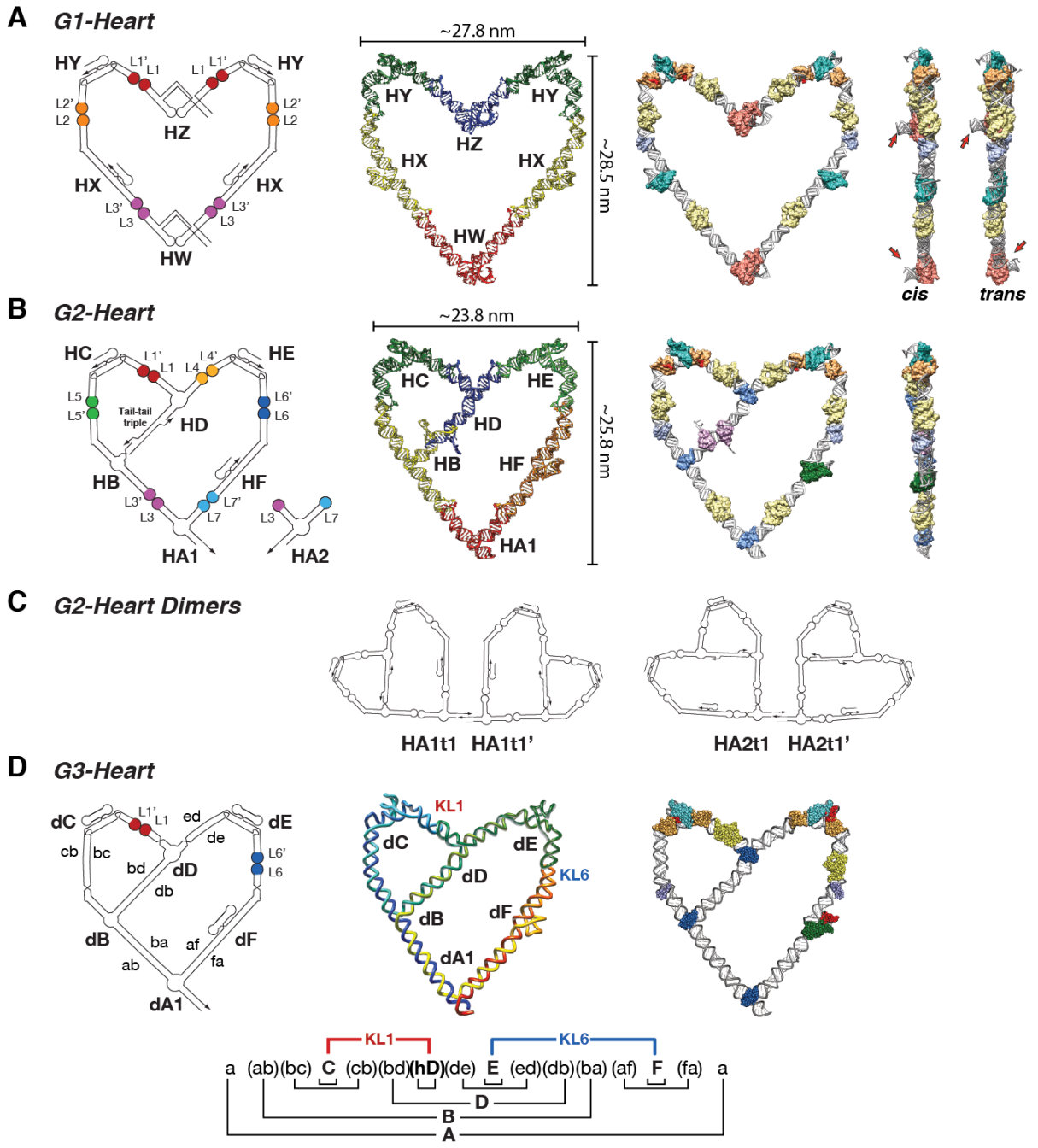

Figure S8: Three-dimensional organization of RNA units and modularity within the hearts of first, second and third generations. (**A**) G1-heart: this 778 nts construct is formed of four different units (HX, HY, HZ, HW) assembling into a 6 units heart with a pseudo-symmetry axis of order 2. It is composed of 7 different RNA structural modules (including the RNA helix). As unit HW and unit HZ can assemble with HY-HX in two different ways, with their 5'-3' ends being oriented on the same (cis) or opposite (trans) side of the heart assembly, two different assembly products are possible. The sides of the cis and trans G1-hearts with the protruding 5'-3' ends are not perfectly flat. Therefore, G1-hearts might not well stick as easily on the mica surface as G2-hearts. (**B**) G2-heart: this 711 nts construct is formed of six different units (HA to HF) that assembles into a fully chiral heart. This heart is composed of 8 different RNA modules (**C**) G2-hearts dimers. The two hearts are linked through a single tail-tail interaction. Corresponding sequences for the G1 and G2 hearts are listed in Table S1. (**D**) G3-heart: this heart is formed of a unique RNA strand folding according to the folding pairing diagram indicated at the bottom of the figure. It is formed of 8 different RNA modules.

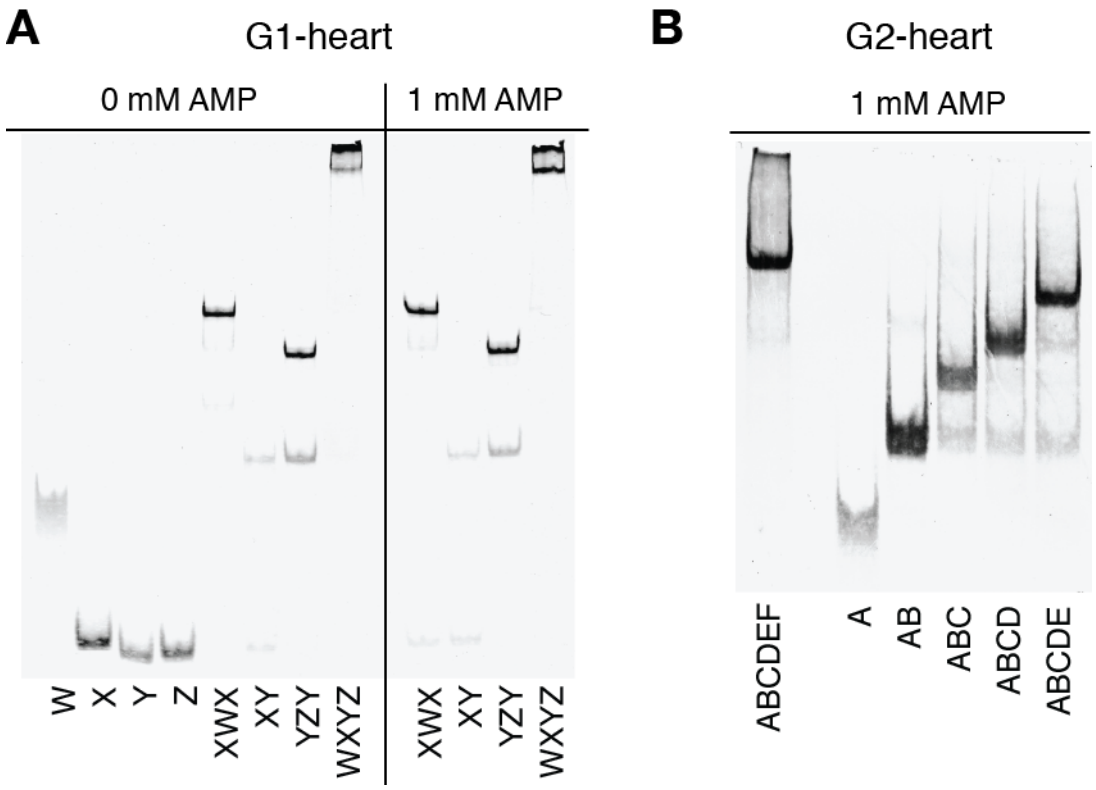

Figure S9: Self-assembly of G1 and G2 hearts in presence of AMP. (**A**) Self-assembly of G1-heart in presence or absence of AMP, visualized by native PAGE at 15 mM $Mg(OAc)_2$ and 10°C, followed by blue staining. (**B**) Self-assembly of G2-heart in presence of AMP visualized by native PAGE at 15 mM $Mg(OAc)_2$ and 10°C, followed by blue staining. Equimolar concentration (100 nM) of RNA units is used for (A) and (B).

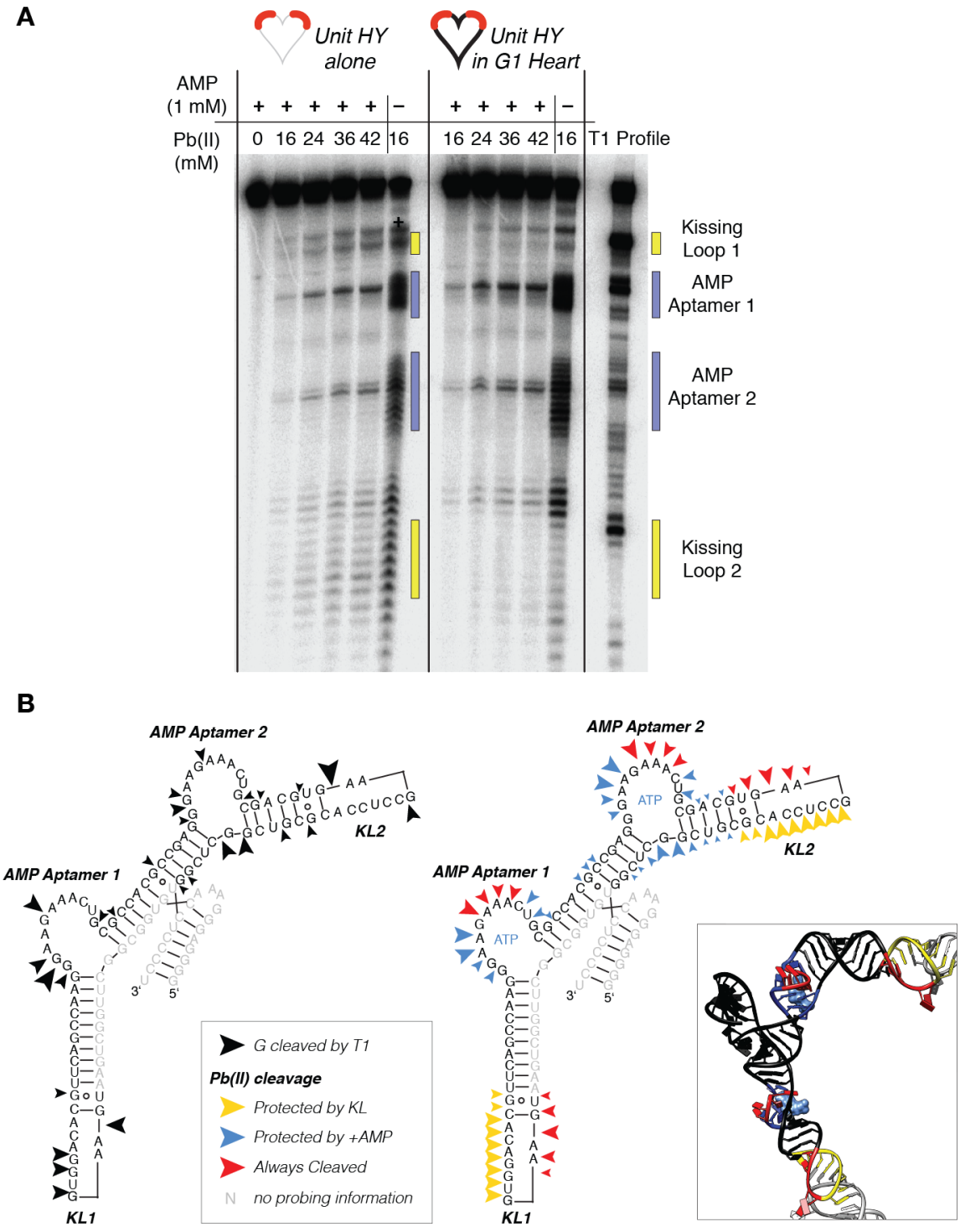

Figure S10: Self-assembly of G1-heart in presence and absence of AMP. Folding of the AMP aptamer module in the context of the unit HY in isolation or within the G1-heart, is monitored by Pb(II) probing in absence and presence of AMP (see Material and Methods). (**A**) The AMP aptamer regions are protected from lead cleavage in presence of AMP in both contexts, indicating that the AMP aptamer modules fold into compact structures upon AMP recognition in both structural contexts. By contrast kissing-loops are only protected in the context of the G1-heart. Profiles shown in Figure 3a correspond to gel lanes at 42 mM Pb(II). (**B**) Pb(II) and Rnase T1 cleavage patterns mapped on the secondary structure diagram of unit HY. T1 cleavage was obtained in absence of AMP.

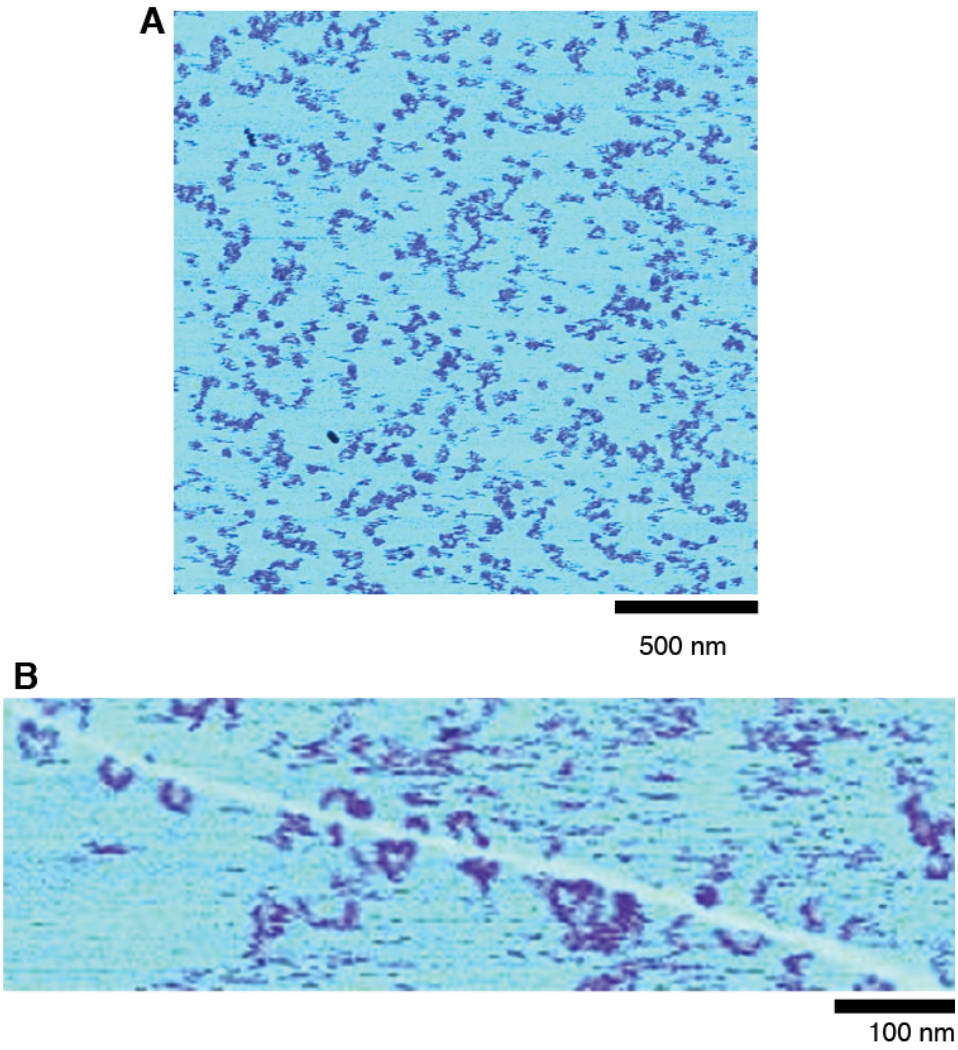

Figure S11: Visualization of G1-hearts by AFM under solution. AFM images of G1-hearts (100 nM) were acquired at 20°C under solution (15 mM $Mg(OAc)_2$, TB buffer) as described in the Material and Methods. (**A**) AFM image showing several discreet RNA particles corresponding to G1-hearts. Imaging of G1-hearts are particularly challenging as they do not stick well on the mica surface and can easily be displaced from the surface by the AFM tip. This might explain the fuzziness of the image. (**B**) Several G1-hearts are seen aligned at the level of a defect on the mica surface. The defect (crack) on the mica likely prevents the hearts to be as easy displaced by the AFM tip under solution.

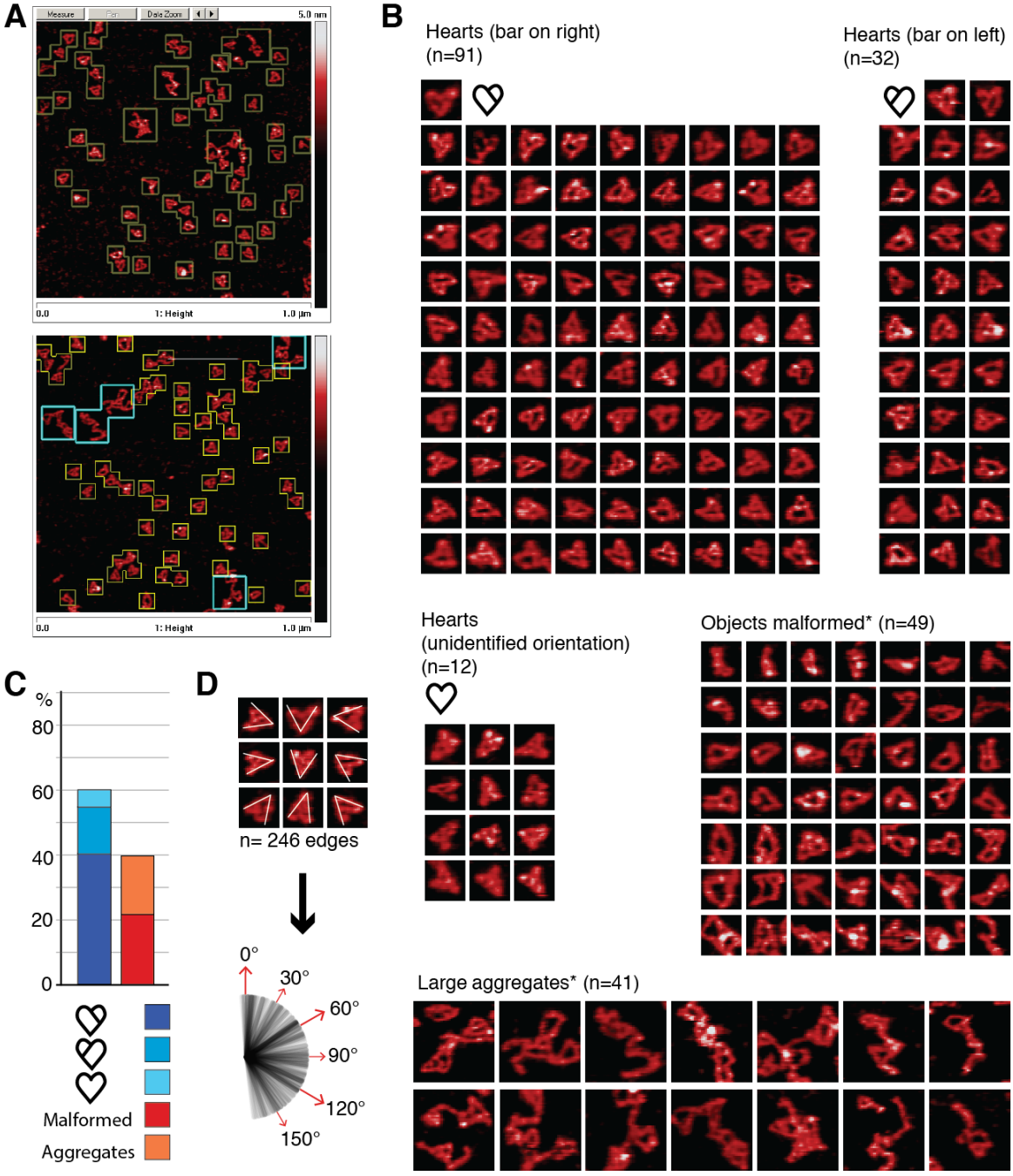

Figure S12: Characterization of G2-hearts by AFM under air (see Materials and Methods). (**A**) Typical AFM images used for the quantitation of hearts immobilized on the mica surface. (**B**) Quantitation of G2-hearts. (*) For malformed objects and large aggregates, the n value corresponds to an estimate of RNA in "equivalent hearts". (**C**) Percent of well-formed hearts versus malformed particles and aggregates. (**D**) The two edges of all G2-hearts with visible inside bar were vectorized and aligned (n=246). A very slight bias in the way these edges bind to the mica surface can be observed, suggesting a small epitaxial effect: the edges partially align with the hexagonal mica lattice. *Additional comments:* 60 % of the RNA on the mica surface corresponds to well-formed G2-hearts. Considering the drying treatment used to image the particles under air, which is likely to be partially denaturing to the particles, this is a low estimate of the yield of well-formed hearts. By native gels, up to 90% of the RNA units assemble into an object that migrates as a single band. The yield of well-formed G2-hearts is closer to 75% when visualized by cryo-EM. The number of G2-hearts with the bar on the right is three times the one of Hearts with the bar on the left, suggesting that G2-hearts adhere better to the mica surface with one of their side. This strong bias observed by AFM likely results from the modality of interactions of RNA with mica. Indeed, by cryo-EM, the proportion of G2-hearts with the bar on the right remains the same as the one with the bar on the left (Fig. S13).

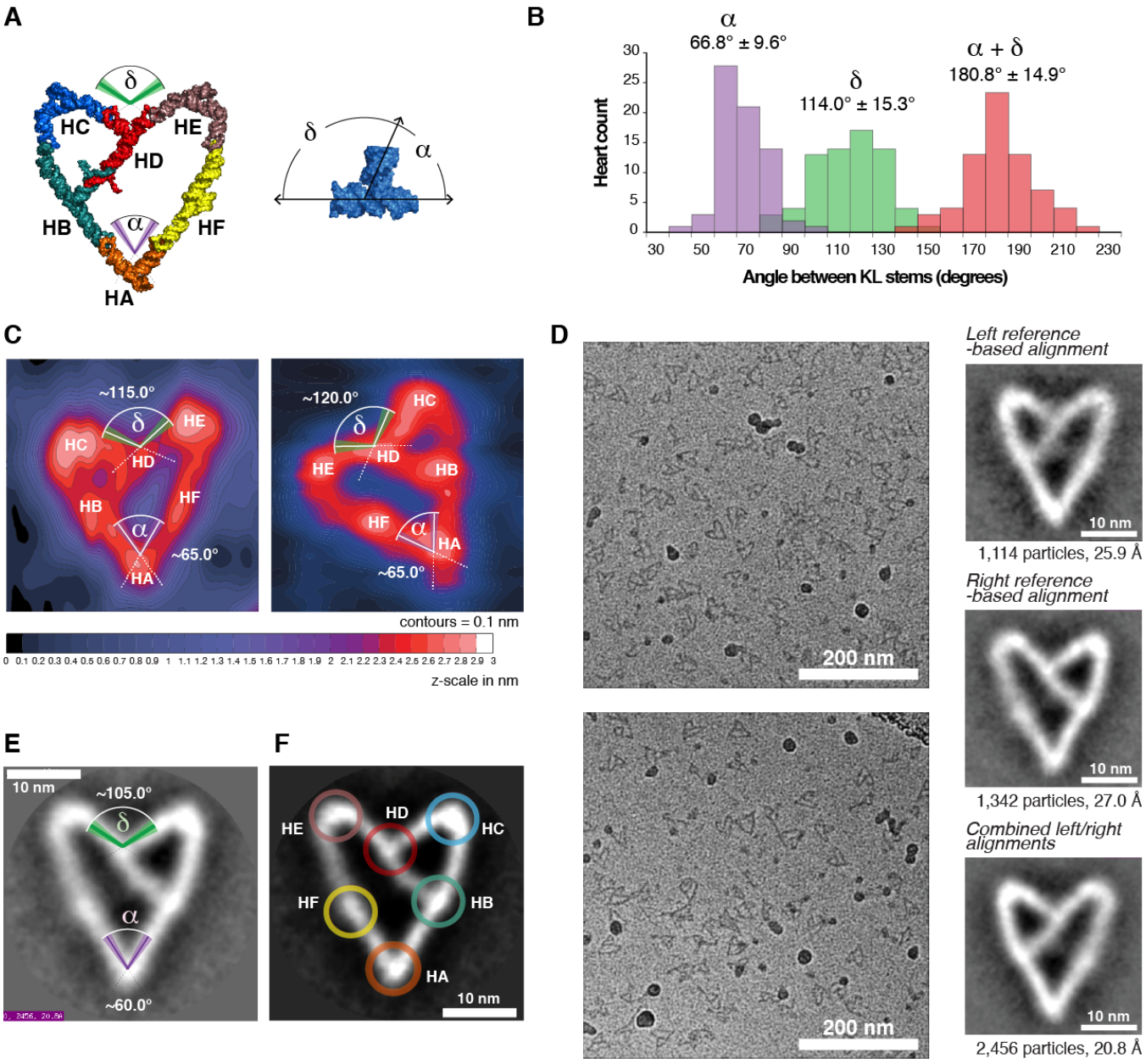

Figure S13: The G2-heart has distinctive structural features dictated by its constituent RNA modules. (**A**) The G2-heart has several kinks and bends specified by the UA_h-3WJ module (on the right: see also Fig. S4). This module orients three helices by an obtuse (δ) and acute (α) angle. (**B**) Distribution of acute and obtuse angles within the population of G2-hearts visualized by AFM. The UA_h-3WJ module presents some degrees of flexibility as also suggested by comparing UA_h-3WJ modules from X-ray structures. (**C**) Two high-resolution AFM images of G2-hearts. Regions with tertiary RNA modules have higher heights than helical regions. Contour plots were generated by interpolation and smoothening of the high resolution AFM images. (**D**) Examples of cryo-EM images for the G2-heart particles with image alignments for a total of 2456 G2-heart particles (see Materials and Methods). (**E, F**) G2-hearts visualized by cryo-EM display similar characteristics as those noticed by AFM. (**E**) Values for δ and α angles are within the same range as those observed by AFM. (**F**) Higher electron densities are observed at the level of RNA tertiary modules within the heart particle.

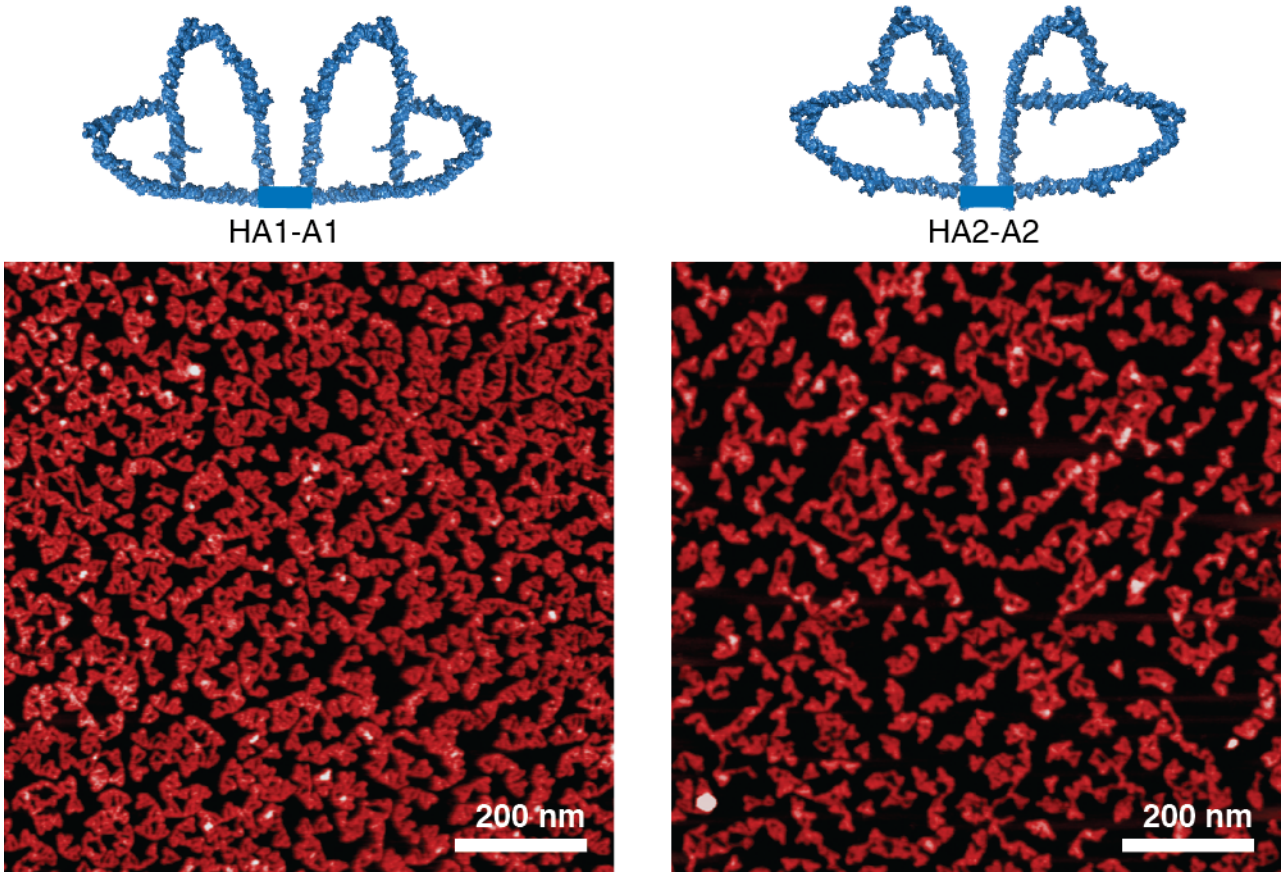

Figure S14: G2-hearts can assemble into dimers through a single tail-tail interaction. AFM images were obtained in air as described in the Materials and Methods. G2-heart dimer samples were assembled in presence of 15 mM $Mg(OAc)_2$ and deposited on the mica surface at a final RNA concentration of 100 nM before drying.

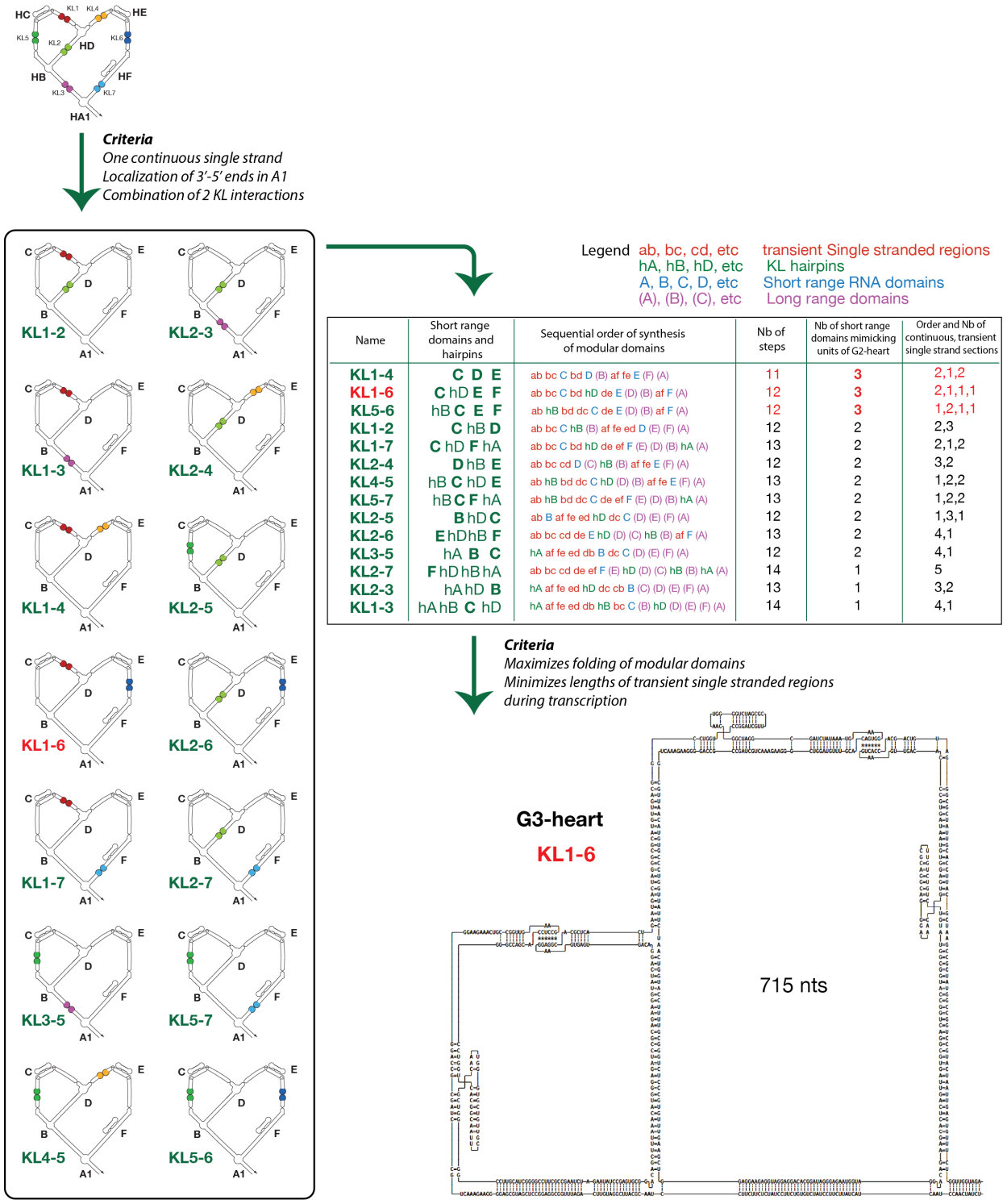

Name	Short range domains and hairpins	Sequential order of synthesis of modular domains	Nb of steps	Nb of short range domains mimicking units of G2-heart	Order and Nb of continuous, transient single strand sections
KL1-4	C D E	ab bc C bd D (B) af fe E (F) (A)	11	3	2,1,2
KL1-6	C hD E F	ab bc C bd hD de E (D) (B) af F (A)	12	3	2,1,1,1
KL5-6	hB C E F	ab hB bd dc C de E (D) (B) af F (A)	12	3	1,2,1,1
KL1-2	C hB D	ab bc C hB (B) af fe ed D (E) (F) (A)	12	2	2,3
KL1-7	C hD F hA	ab bc C bd hD de ef F (E) (D) (B) hA (A)	13	2	2,1,2
KL2-4	D hB E	ab bc cd D (C) hB (B) af fe E (F) (A)	12	2	3,2
KL4-5	hB C hD E	ab hB bd dc C hD (D) (B) af fe E (F) (A)	13	2	1,2,2
KL5-7	hB C F hA	ab hB bd dc C de ef F (E) (D) (B) hA (A)	13	2	1,2,2
KL2-5	B hD C	ab B af fe ed hD dc C (D) (E) (F) (A)	12	2	1,3,1
KL2-6	E hD hB F	ab bc cd de E hD (D) (C) hB (B) af F (A)	13	2	4,1
KL3-5	hA B C	hA af fe ed db B dc C (D) (E) (F) (A)	12	2	4,1
KL2-7	F hD hB hA	ab bc cd de ef F (E) hD (D) (C) hB (B) hA (A)	14	1	5
KL2-3	hA hD B	hA af fe ed hD dc cb B (C) (D) (E) (F) (A)	13	1	3,2
KL1-3	hA hB C hD	hA af fe ed db hB bc C (B) hD (D) (E) (F) (A)	14	1	4,1

Figure S15: Criteria used for designing the single stranded G3-heart for co-transcriptional folding. Using the indicated design criteria, fourteen different folding pathways can be anticipated. Among the three pathways (KL1-4, KL1-6, KL5-6) that maximize the folding of short-range modular domains corresponding to G2-heart units, the KL1-6 pathway is potentially conducive to the early folding of one of its constituent RNA domains during transcription (like KL1-4, KL1-2, KL1-7, KL2-5) and also minimizes the occurrence of long single stranded regions during transcription (like KL5-6). The 2D structure of G3-heart is shown.

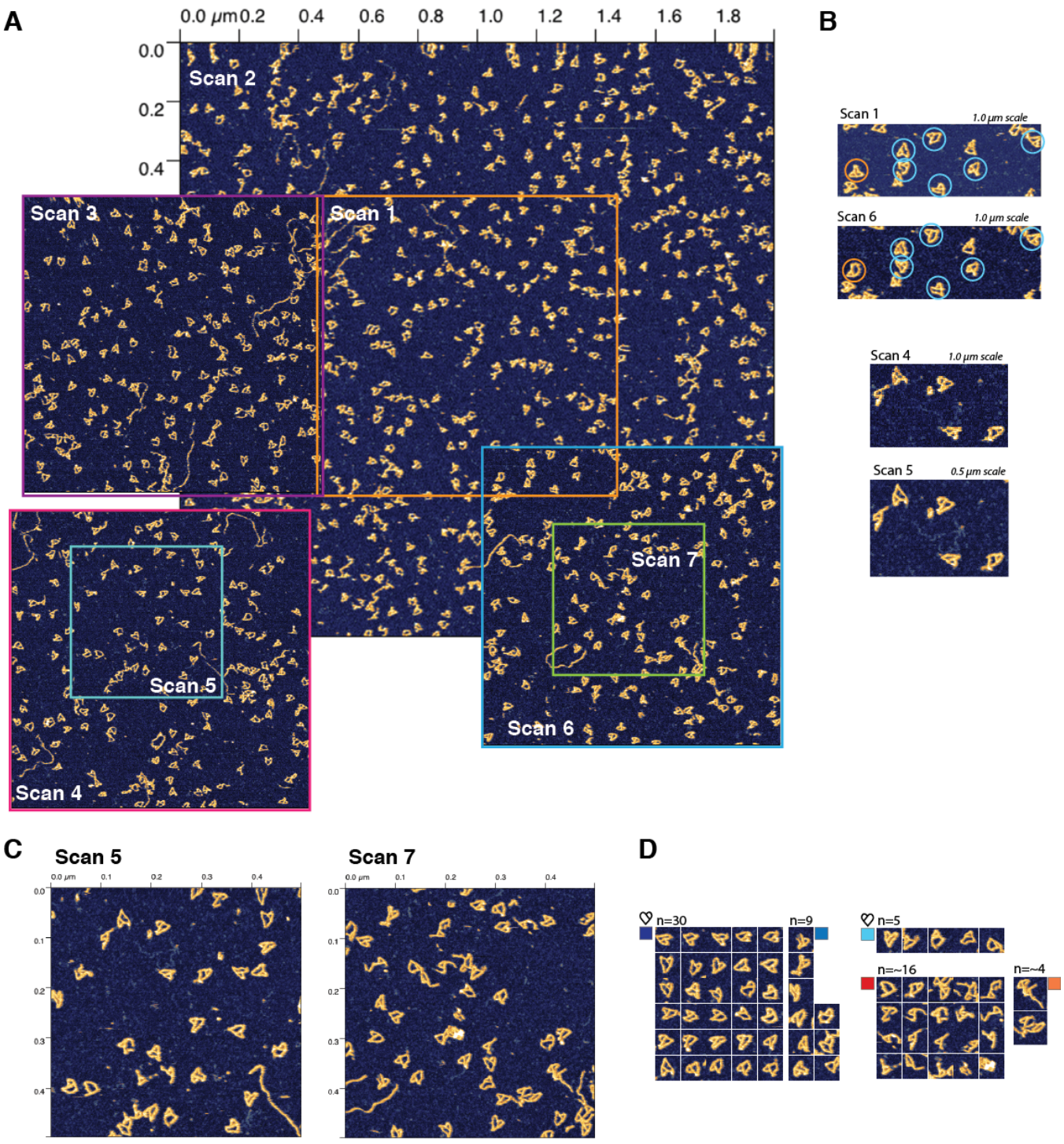

Figure S16: Single stranded G3-hearts can efficiently be generated during transcription in isothermal conditions. (**A**) Various AFM images of G3-hearts obtained under solution as described in the Materials and Methods sections. (**B**) Details of regions scanned twice by AFM. Most hearts do not change much in shape. A few hearts, which seem to be broken or deformed on the first scan, display nice heart shapes on the last scan (see hearts circled in blue). This suggests that apparent brokenness might be artifacts of AFM. Nevertheless, a few hearts are also observed to be disrupted by the AFM tip (see heart circled in red). **(C, D)** Higher resolution images reveal nicer heart shapes. (**C**) 0.5 µm scale AFM images used for quantitating RNA objects with heart shapes (**D**). See also Figure 4d.

4. Supplementary References

(1) Severcan, I.; Geary, C.; Verzemnieks, E.; Chworos, A.; Jaeger, L. *Nano Lett.* **2009,** 9, 1270-1277.
(2) Severcan, I.; Geary, C.; Chworos, A.; Voss, N.; Jacovetty, E.; Jaeger, L. *Nat. Chem.* **2010,** 2, 772-9.
(3) Suloway, C.; Pulokas, J.; Fellmann, D.; Cheng, A.; Guerra, F.; Quispe, J.; Stagg, S.; Potter, C. S.; Carragher, B. *J. Struct. Biol.* **2005,** 151, 41-60.
(4) Lander, G. C.; Stagg, S. M.; Voss, N. R.; Cheng, A.; Fellmann, D.; Pulokas, J.; Yoshioka, C.; Irving, C.; Mulder, A.; Lau, P.-W.; Lyumkis, D.; Potter, C. S.; Carragher, B. *J. Struct. Biol.* **2009,** 166, 95-102.
(5) Roseman, A. M. *Ultramicroscopy* **2003,** 94, 225-36.
(6) Mallick, S. P.; Carragher, B.; Potter, C. S.; Kriegman, D. J. *Ultramicroscopy* **2005,** 104, (1), 8-29.
(7) Voss, N. R.; Lyumkis, D.; Cheng, A.; Lau, P. W.; Mulder, A.; Lander, G. C.; Brignole, E. J.; Fellmann, D.; Irving, C.; Jacovetty, E. L.; Leung, A.; Pulokas, J.; Quispe, J. D.; Winkler, H.; Yoshioka, C.; Carragher, B.; Potter, C. S. *J. Struct. Biol.* **2010,** 169, 389-98.
(8) Scheres, S. H. W.; Valle, M.; Carazo, J. e. M. i. a. *Bioinformatics* **2005,** 21 Suppl 2, ii243-4.
(9) Scheres, S. H. W.; Valle, M.; Grob, P.; Nogales, E.; Carazo, J. M. *J. Struct. Biol.* **2009,** 166, 234-40.
(10) Unser, M.; Trus, B. L.; Steven, A. C. *Ultramicroscopy* **1987,** 23, 39-51.
(11) Geary, C.; Chworos, A.; Jaeger, L. *Nucleic Acids Res.* **2011,** 39, 1066-80.
(12) Leontis, N. B.; Westhof, E. *RNA* **2001,** 7, 499-512.
(13) Jaeger, L.; Verzemnieks, E. J.; Geary, C. *Nucleic Acids Res.* **2009,** 37, 215--230.
(14) Grabow, W. W.; Zhuang, Z.; Shea, J. E.; Jaeger, L. *Wiley Interdiscip Rev. RNA* **2013,** 4, 181-203.